Nano-Hexapod on the micro-station

Dehaeze Thomas

March 19, 2024

Contents

1 Short Stroke Metrology System

The control of the nano-hexapod requires an external metrology system measuring the relative position of the nano-hexapod top platform with respect to the granite. As the long-stroke ($\approx 1\,cm^3$) metrology system is not developed yet, a stroke stroke ($> 100\,\mu m^3$) can be used instead to validate the nano-hexapod control.

This short stroke metrology system consists of 5 interferometers pointing at 2 spheres fixed on top of the nano-hexapod (Figure 1.1).

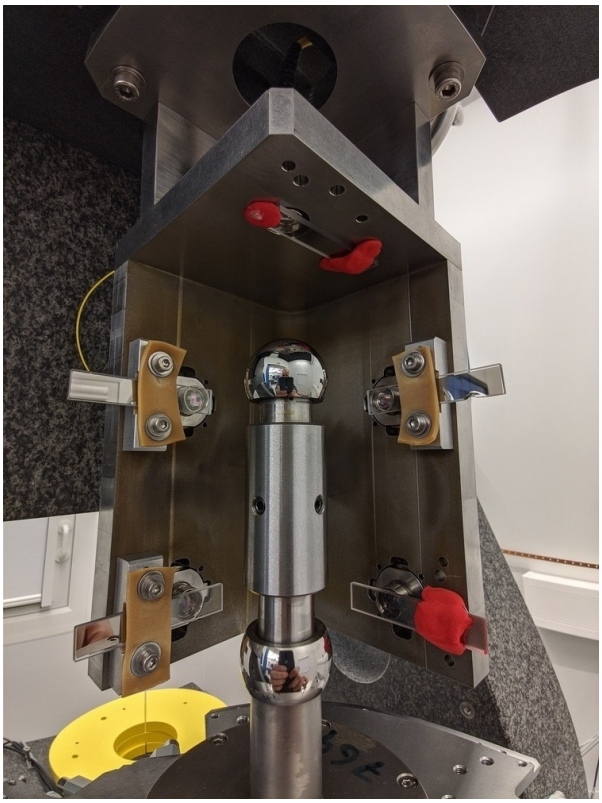

Figure 1.1: Metrology system with LION spheres (1 inch diameter) and 5 interferometers fixed to their individual tip-tilts

This short stroke metrology system is fixed to the main granite using a gantry made of granite blocs to have good vibration and thermal stability (see Figure 1.2).

As the metrology system as limited stroke (estimated to be in the order of hundreds of micro-meters in x-y-z), it has to be well aligned in the rest position.

The alignment procedure is as follows:

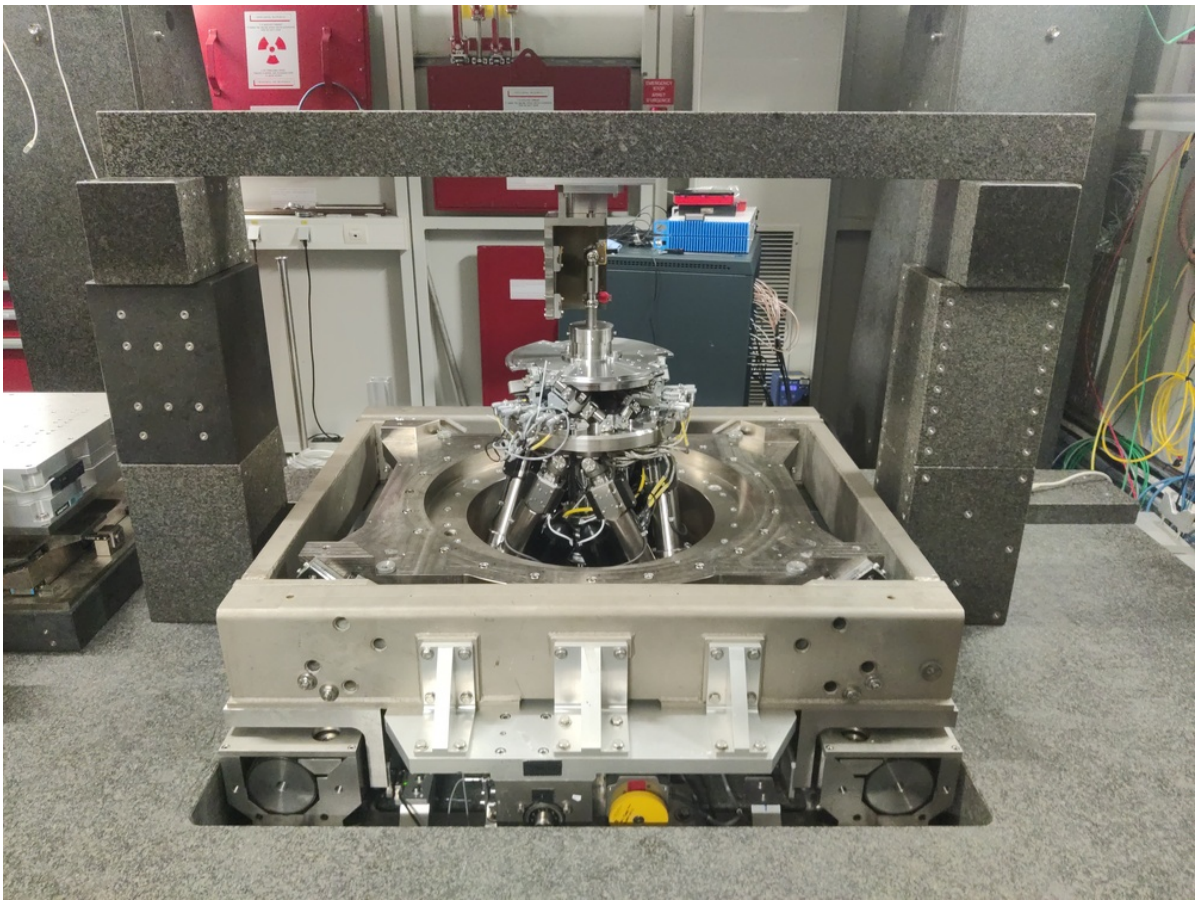

Figure 1.2: Granite gantry used to fix the short-stroke metrology system

1. The granite is aligned to be perpendicular to gravity (using inclinometer and adjusting airlocks)

2. The height of micro-hexapod is tuned to be able to position the short stroke metrology without additional shim

3. It is verified that the spindle axis is well perpendicular to the granite using the laser tracker

4. The micro hexapod is then used to align the two spheres with the spindle axis.

1.1 Kinematics

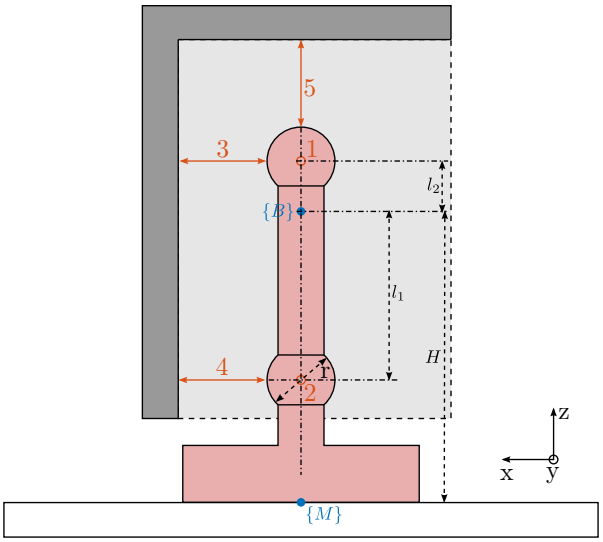

Figure 1.3: Schematic of the measurement system

We have the following set of equations:

$$d_1 = +D_y - l_2 R_x \tag{1.1}$$
$$d_2 = +D_y + l_1 R_x \tag{1.2}$$
$$d_3 = -D_x - l_2 R_y \tag{1.3}$$
$$d_4 = -D_x + l_1 R_y \tag{1.4}$$
$$d_5 = -D_z \tag{1.5}$$

That can be written as a linear transformation:

$$\begin{bmatrix} d_1 \\ d_2 \\ d_3 \\ d_4 \\ d_5 \end{bmatrix} = \begin{bmatrix} 0 & 1 & 0 & -l_2 & 0 \\ 0 & 1 & 0 & l_1 & 0 \\ -1 & 0 & 0 & 0 & -l_2 \\ -1 & 0 & 0 & 0 & l_1 \\ 0 & 0 & -1 & 0 & 0 \end{bmatrix} \cdot \begin{bmatrix} D_x \\ D_y \\ D_z \\ R_x \\ R_y \end{bmatrix} \tag{1.6}$$

By inverting the matrix, we obtain the Jacobian relation:

$$\begin{bmatrix} D_x \\ D_y \\ D_z \\ R_x \\ R_y \end{bmatrix} = \begin{bmatrix} 0 & 1 & 0 & -l_2 & 0 \\ 0 & 1 & 0 & l_1 & 0 \\ -1 & 0 & 0 & 0 & -l_2 \\ -1 & 0 & 0 & 0 & l_1 \\ 0 & 0 & -1 & 0 & 0 \end{bmatrix}^{-1} \cdot \begin{bmatrix} d_1 \\ d_2 \\ d_3 \\ d_4 \\ d_5 \end{bmatrix} \tag{1.7}$$

Table 1.1: Jacobian matrix for the metrology system

	d1	**d2**	**d3**	**d4**	**d5**
Dx	0.0	0.0	-0.79	-0.21	0.0
Dy	0.79	0.21	0.0	0.0	0.0
Dz	0.0	0.0	0.0	0.0	-1.0
Rx	-13.12	13.12	-0.0	0.0	0.0
Ry	-0.0	-0.0	-13.12	13.12	0.0

1.2 Rough alignment of spheres using comparators

Bottom Sphere, then top sphere.

Alignment better than 10um. But the coaxiality between the cylinder and the sphere might not be good.

1.3 Alignment of spheres using interferometers

1.3.1 Angular alignment

1.3.2 Eccentricity alignment

1.4 Residual error after alignment

- Dx and Dy are less than 1um.
- Dz less than 0.1um.
- Rx and Ry less than 4urad.

1.5 Metrology acceptance

Because the interferometers are pointing to spheres and not flat surfaces, the lateral acceptance is limited.

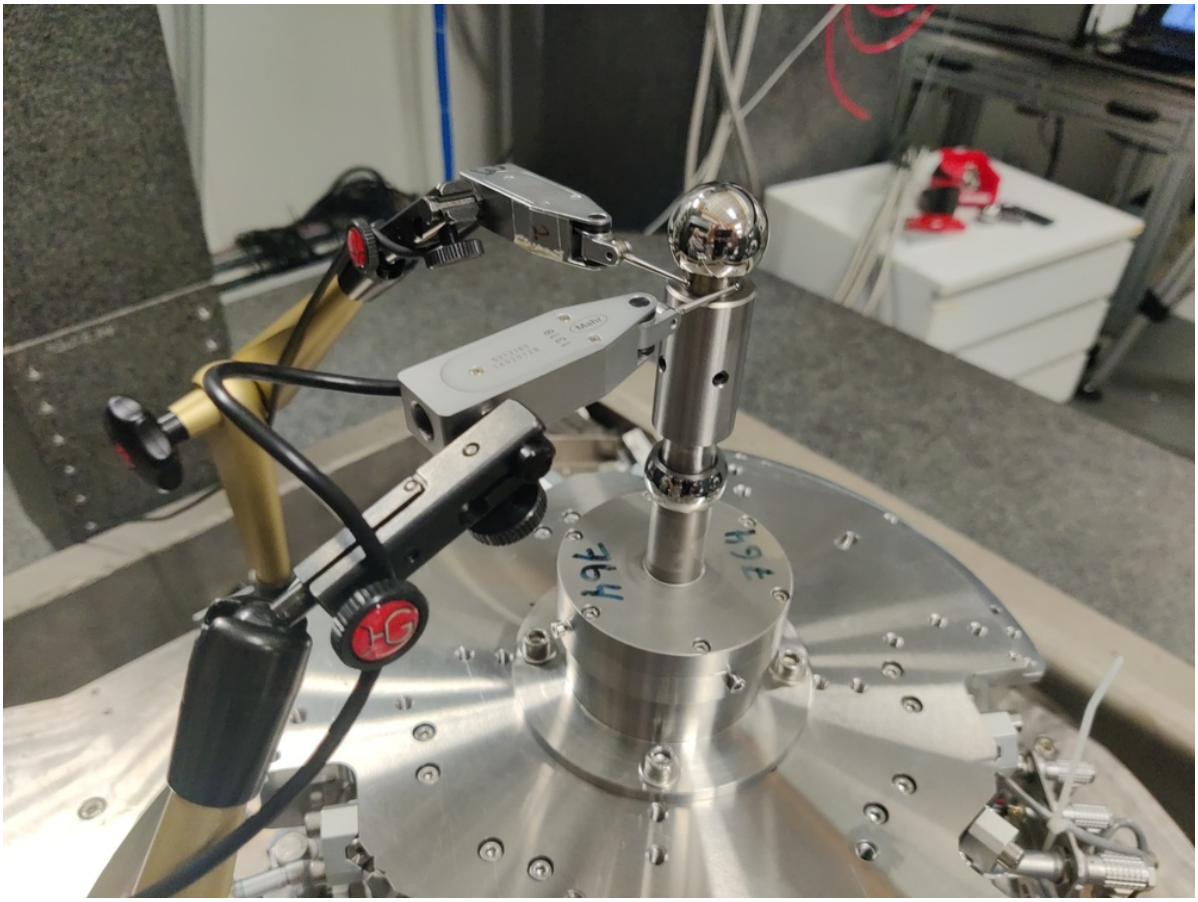

Figure 1.4: Two mechanical comparators used to align the top sphere with the rotation axis of the spindle

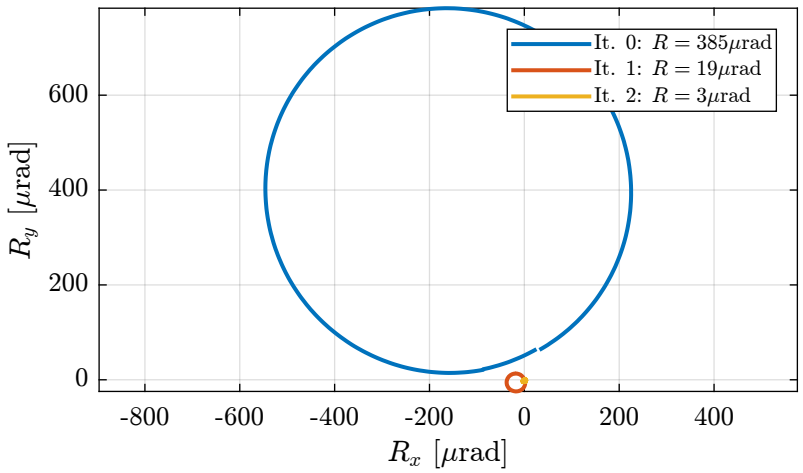

Figure 1.5: Rx/Ry alignment of the spheres using the micro-station

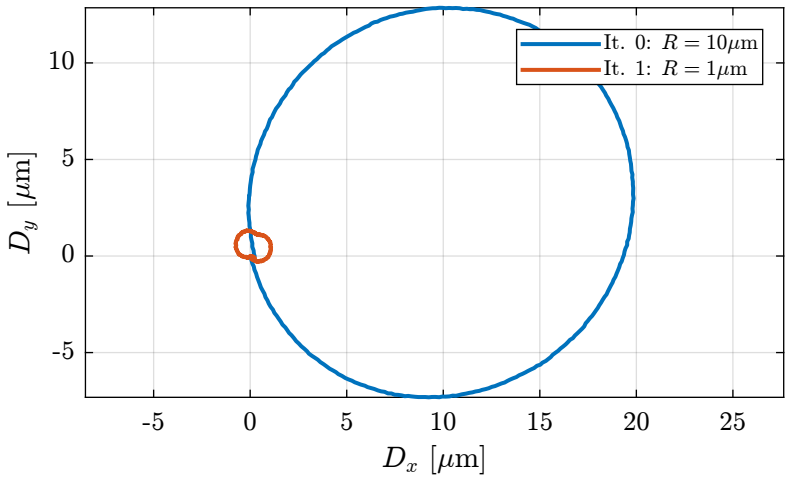

Figure 1.6: Dx/Dy alignment of the spheres using the micro-station

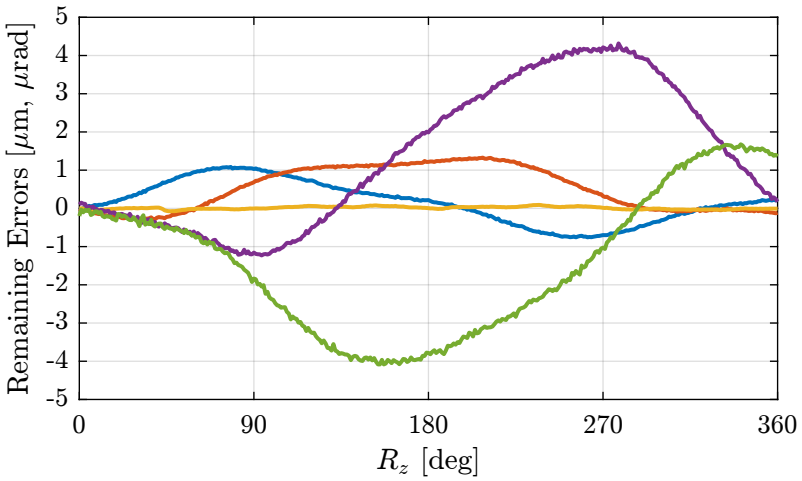

Figure 1.7: Remaining errors after aligning the metrology using the interferometers

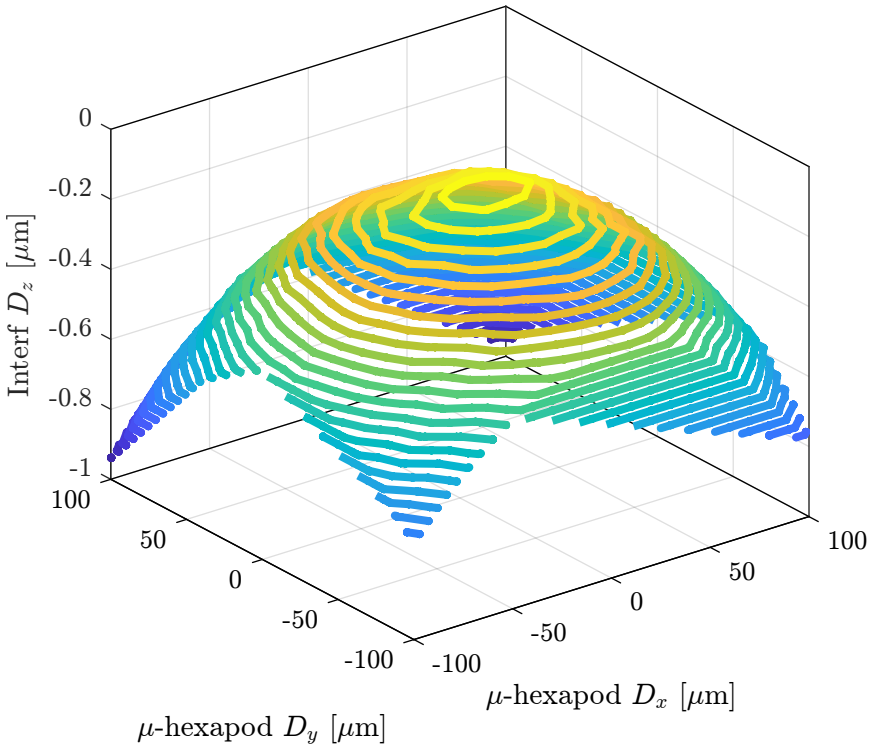

Figure 1.8: XY mapping of the Z measurement by the interferometer

2 Simscape Model

2.1 Init model

2.2 Identify Transfer functions

2.3 IFF Plant

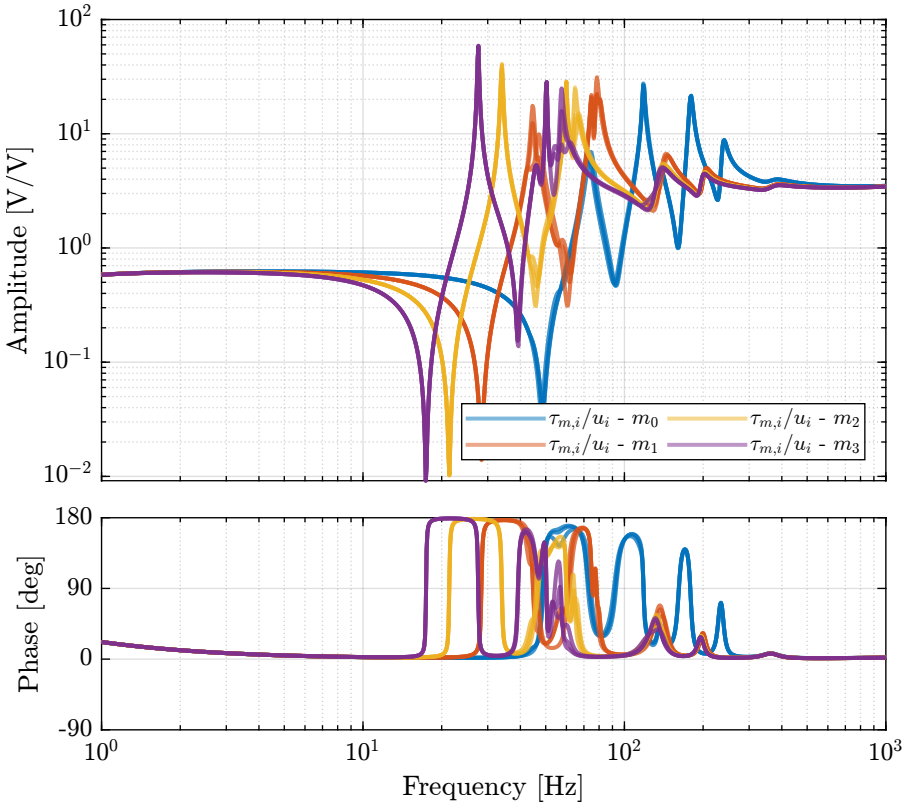

Figure 2.1: IFF transfer function - Simscape model

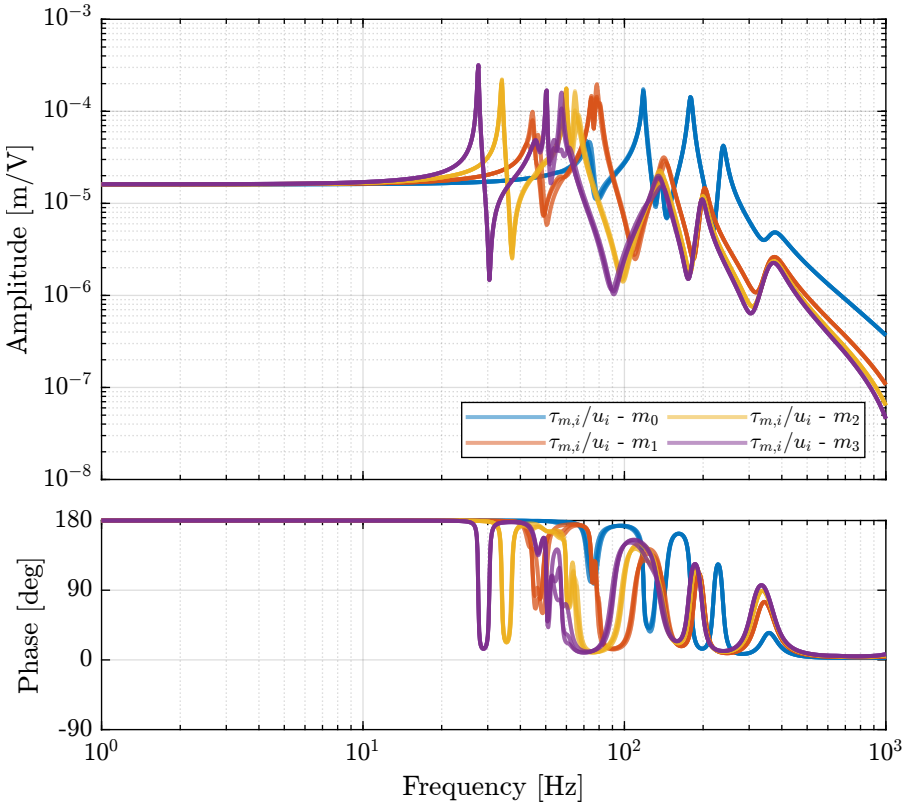

Figure 2.2: ENC transfer function - Simscape model

2.4 Encoder plant

2.5 HAC Undamped plant

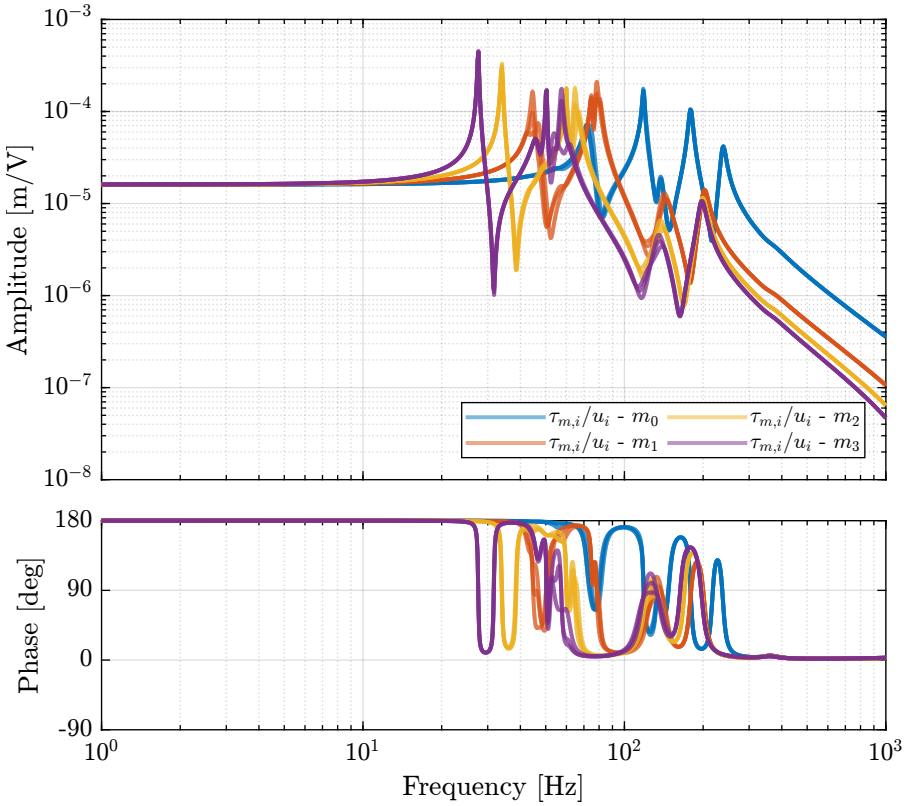

Figure 2.3: INT transfer function - Simscape model

3 Identified Open Loop Plant

3.1 IFF Plant

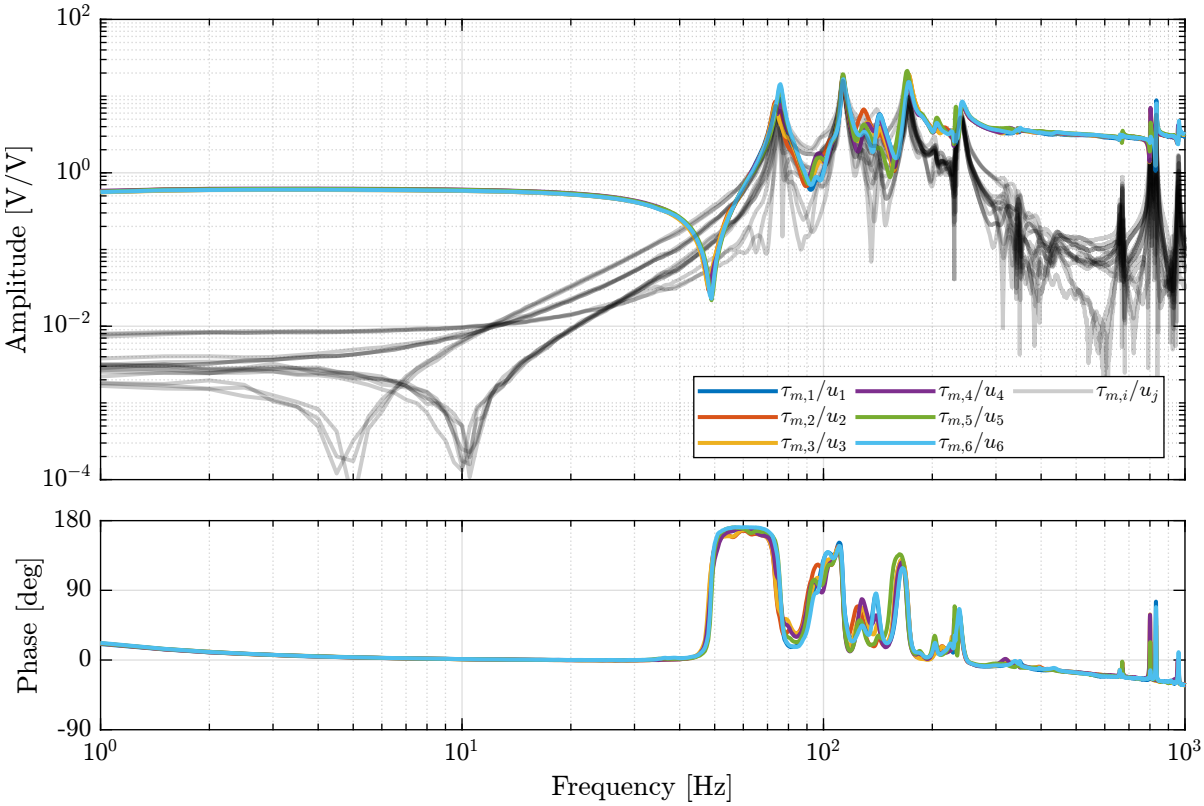

Figure 3.1: Measured transfer function from generated voltages to measured voltage on the force sensors

The measured frequency response functions from DAC voltages u_i to measured voltages on the force sensors $\tau_{m,i}$ are compared with the simscape model in Figure 3.2.

The effect of the payload mass on the diagonal elements are shown in Figure 3.3.

3.2 Encoder plant

The identified frequency response functions from general voltages u_i to measured displacement of the struts by the encoders $d\mathcal{L}_i$ are compared with the simscape model in Figure 3.4.

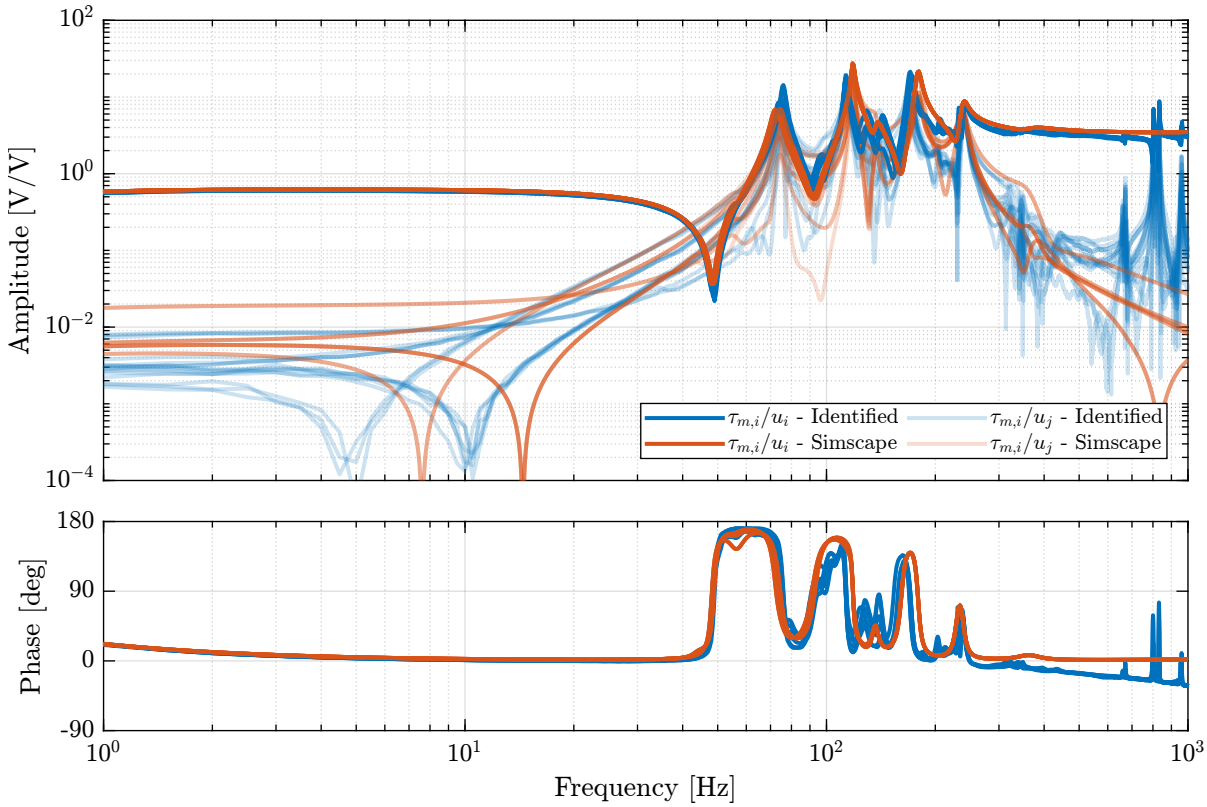

Figure 3.2: Comparison of the Simscape model and identified IFF plant

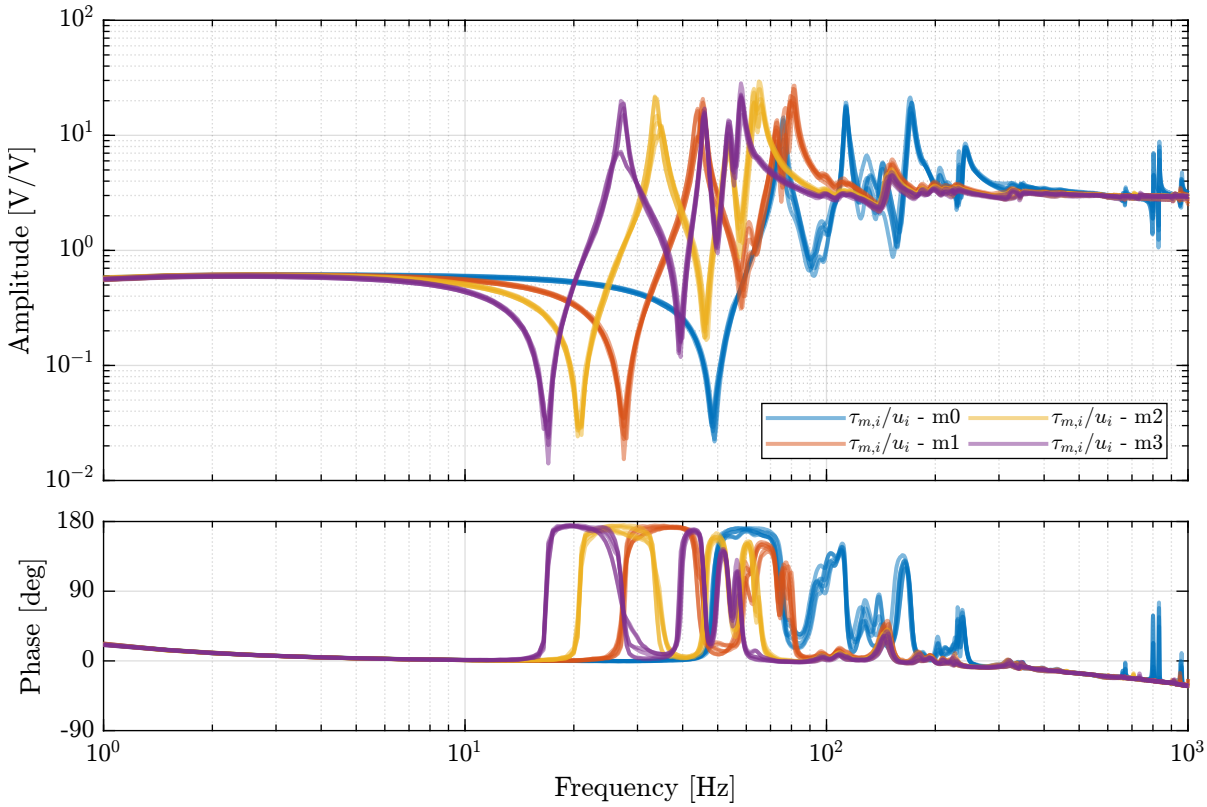

Figure 3.3: Effect of the payload mass on the IFF plant

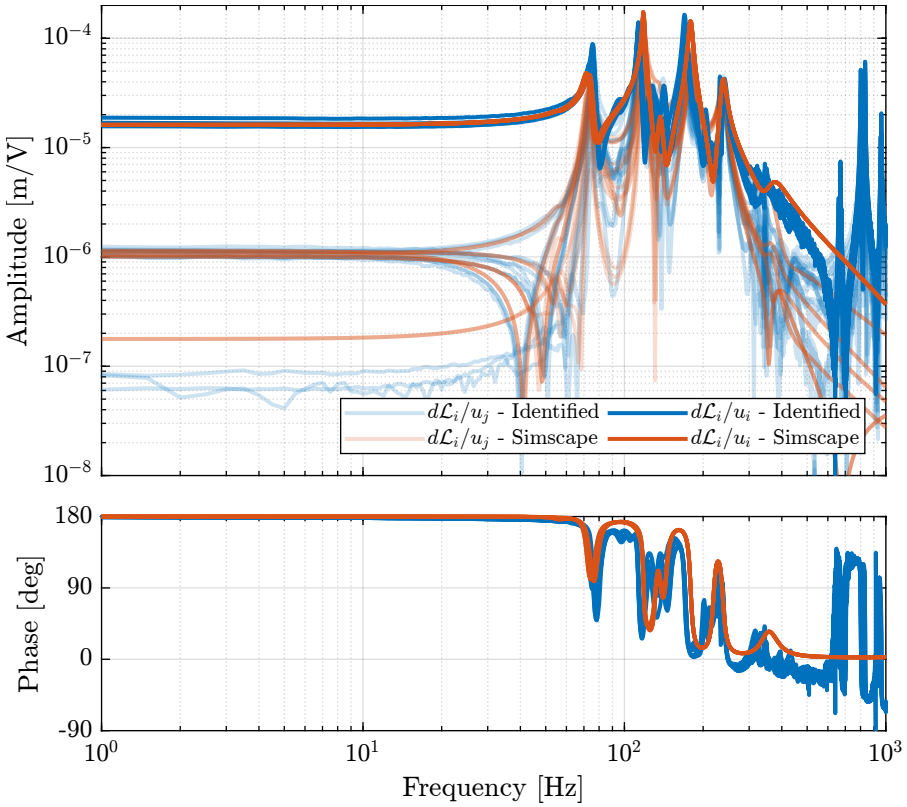

Figure 3.4: Comparison of the Simscape model and identified plant - Transfer functions from voltages to encoders

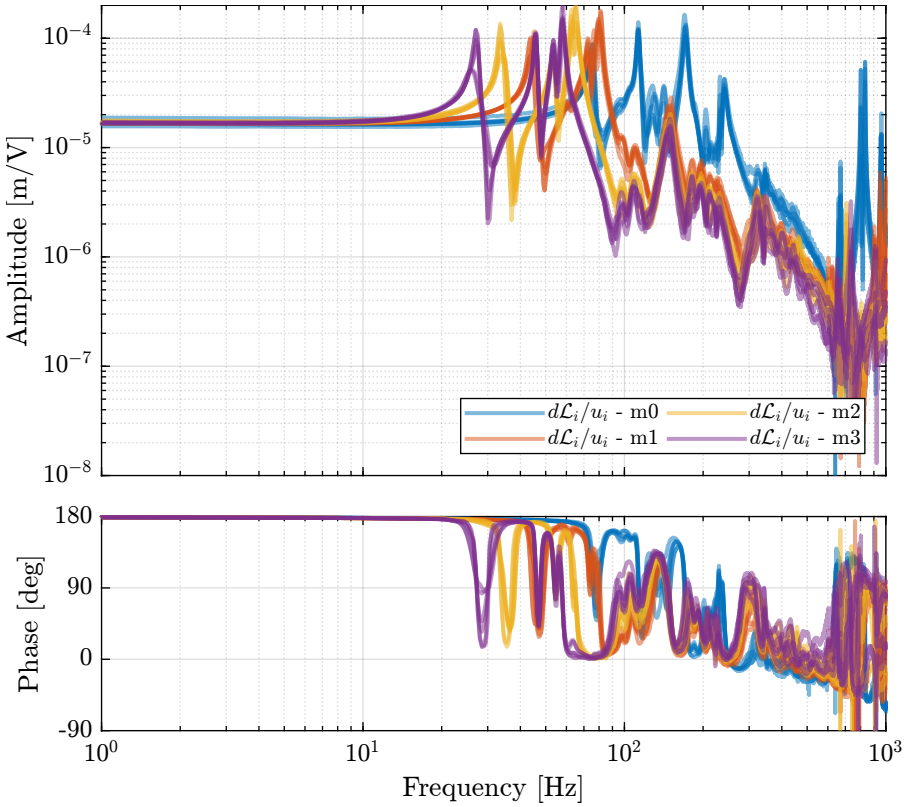

Figure 3.5: Effect of the payload mass on the transfer function from actuator voltage to encoder displacement

3.3 HAC Undamped plant

The identified frequency response functions from actuator voltages u_i to measured strut motion from the external metrology (i.e. the interferometers) are compare with the simscape model in Figure 3.7.

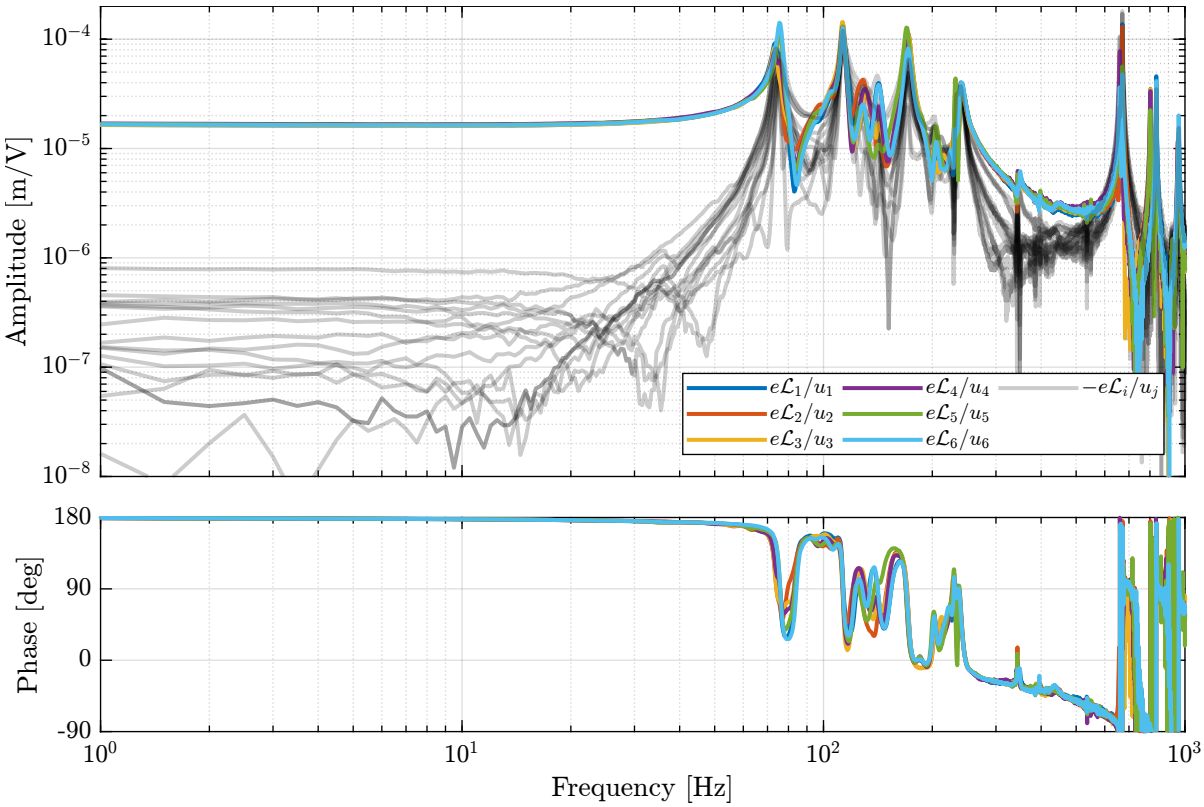

Figure 3.6: Measured transfer function from generated voltages to measured voltage on the force sensors

3.4 Decoupling improvement thanks to better Rz alignment

3.4.1 Alignment procedure

- Control based on encoders
- Slow moving in X and Y
- Compare with X and Y from interf

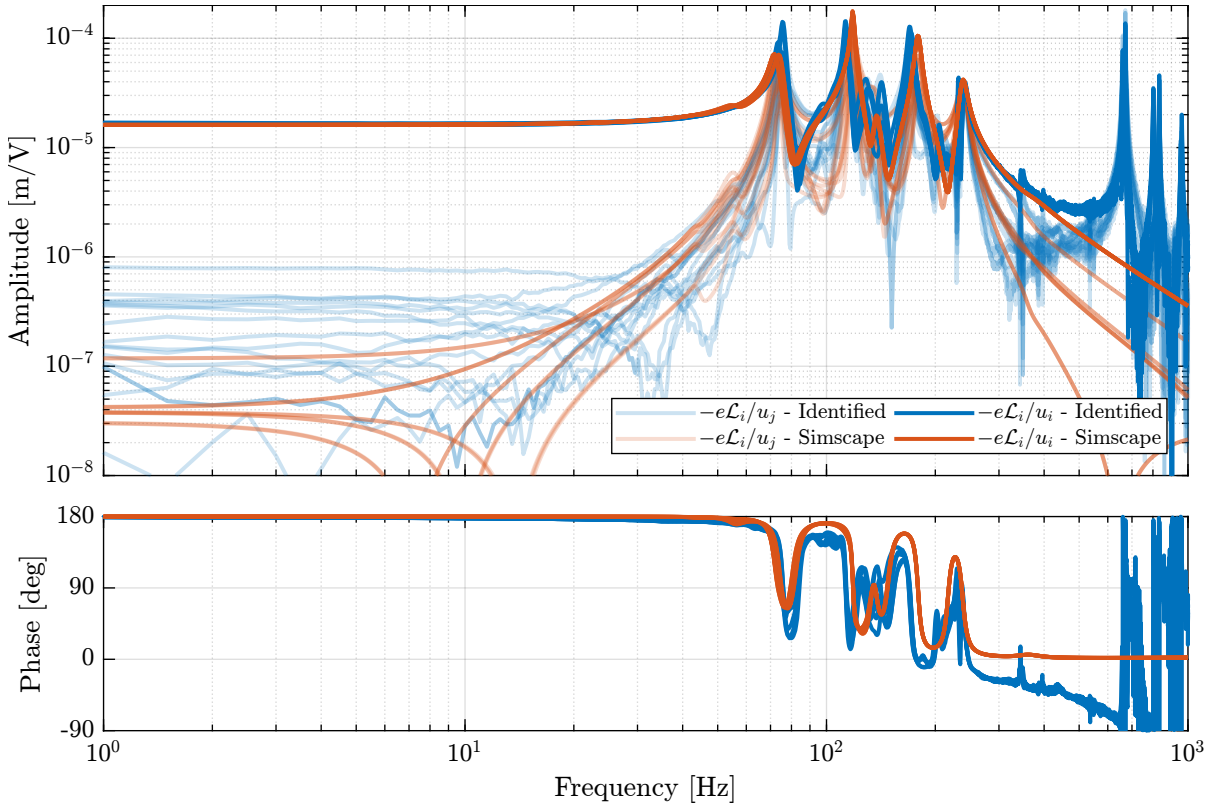

Figure 3.7: Comparison of the Simscape model and identified plant - Transfer functions from voltages to estimated strut motion from interferometers

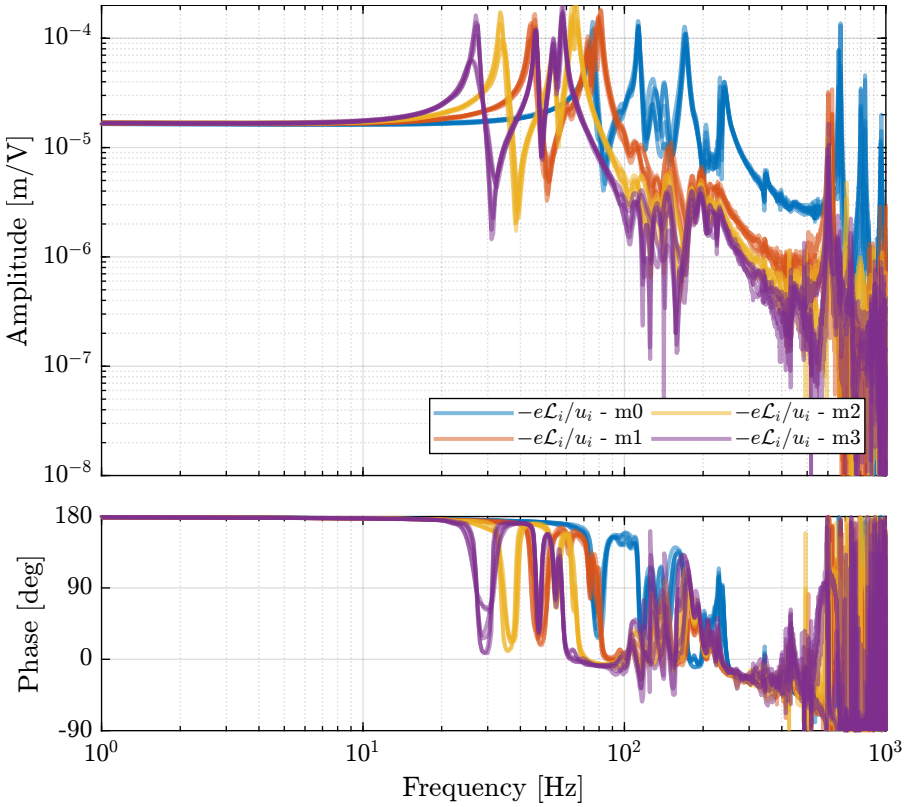

Figure 3.8: Effect of the payload mass on the transfer functions from actuator voltage to measured strut motion by the external metrology

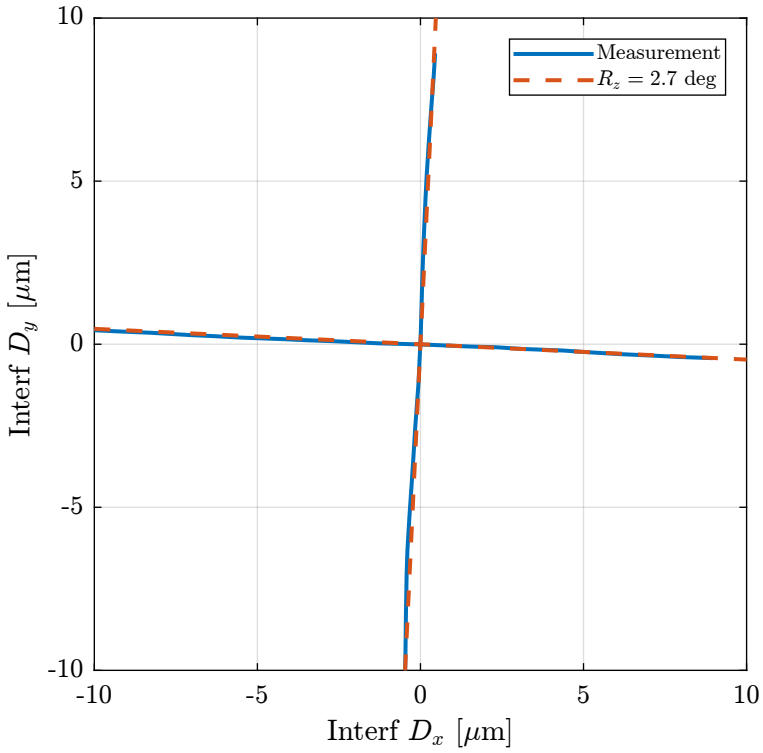

Figure 3.9: description

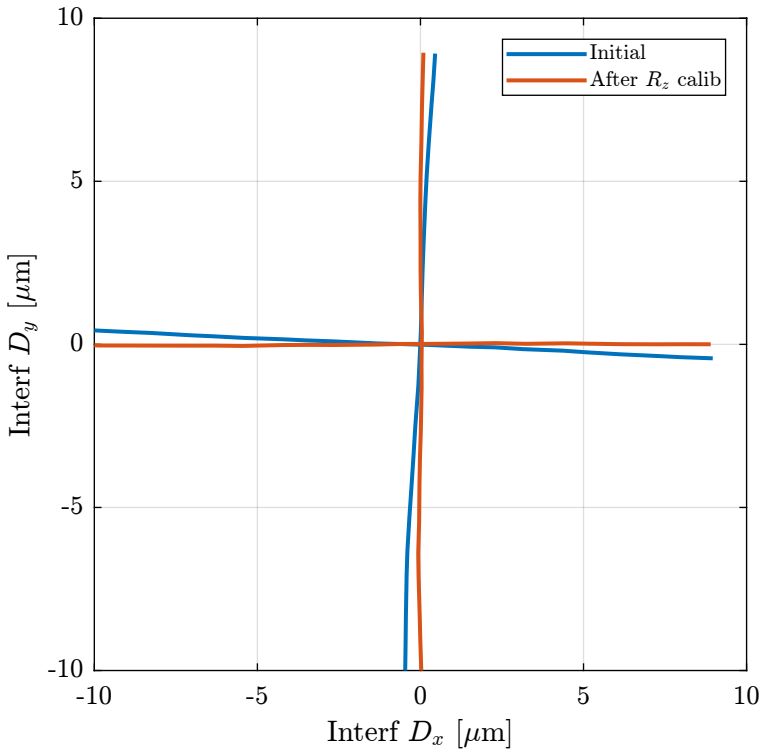

Figure 3.10: description

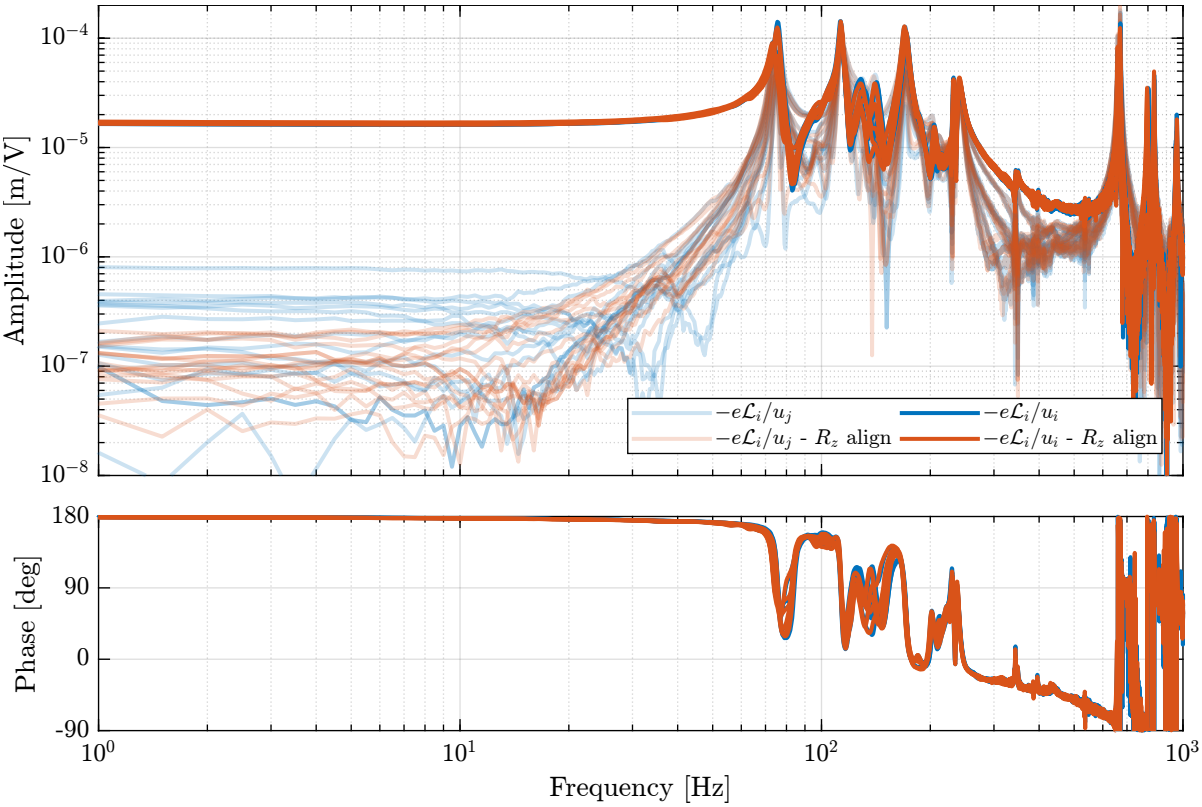

Figure 3.11: Decrease of the coupling with better Rz alignment

3.4.2 m0

3.4.3 m3

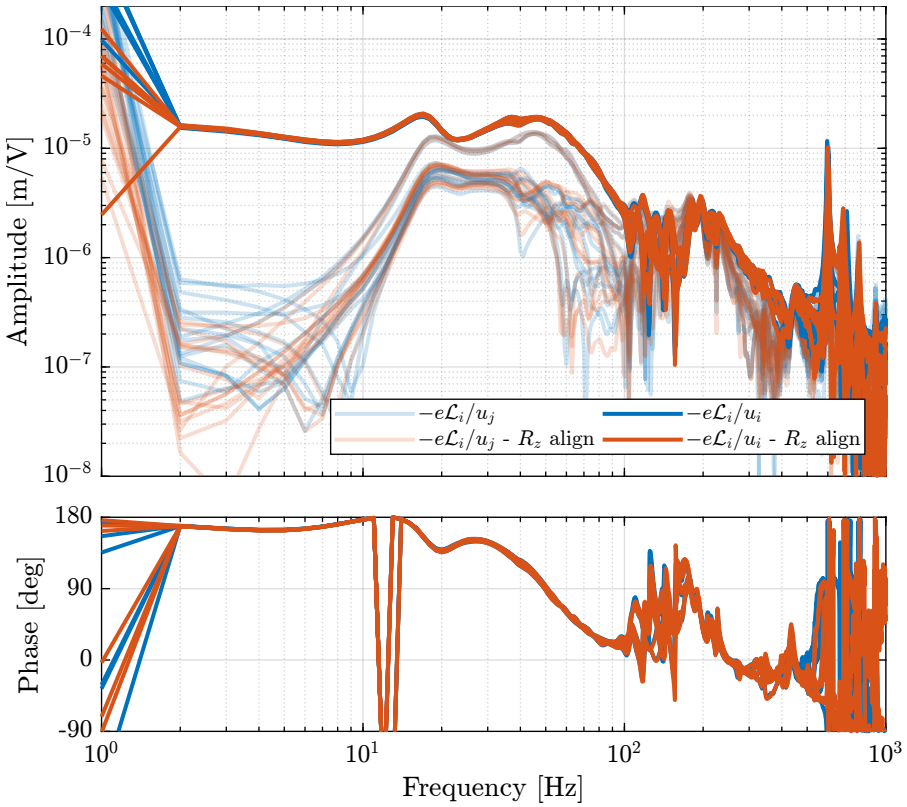

Figure 3.12: Decrease of the coupling with better Rz alignment

3.5 Conclusion

- Good match between the model and experiment

4 Noise Budget

In this section, the noise budget is performed. The vibrations of the sample is measured in different conditions using the external metrology.

4.1 Open-Loop Noise Budget

First, the noise is measured while no motion is performed.

Noise budget in the cartesian frame Data in the time domain

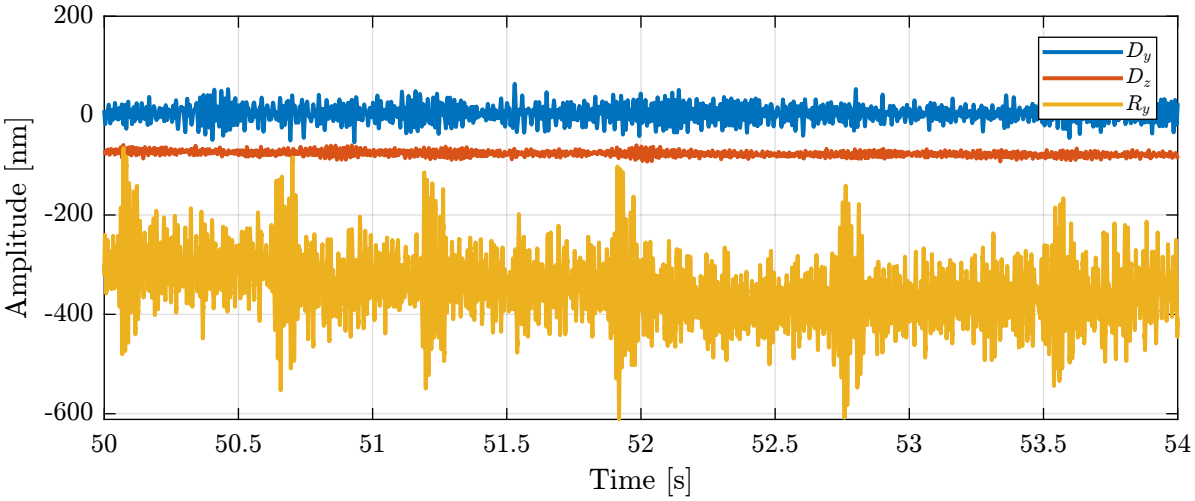

Figure 4.1: Measured vibration with the interferometers

In the frequency domain

4.2 Effect of LAC

Effect of LAC (Figure 4.4):

- reduce amplitude around 80Hz
- Inject some noise between 200 and 700Hz?

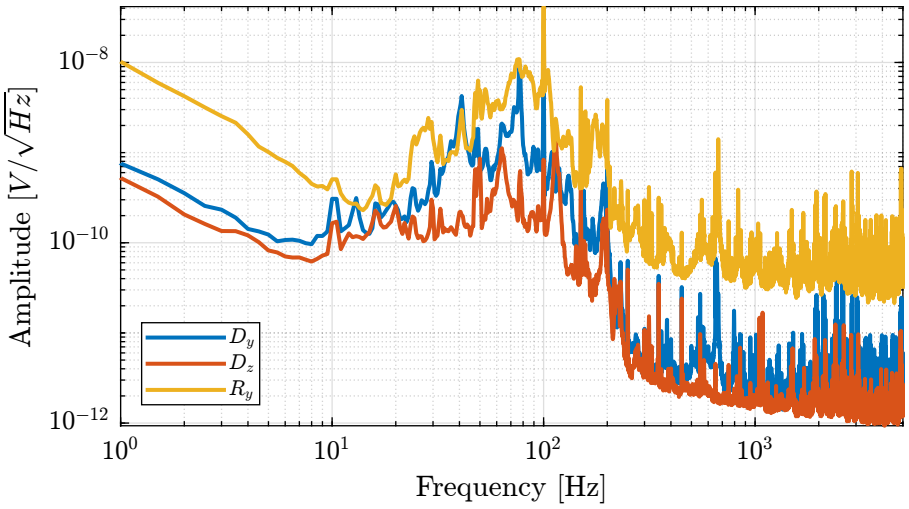

Figure 4.2: Measured vibration with the interferometers

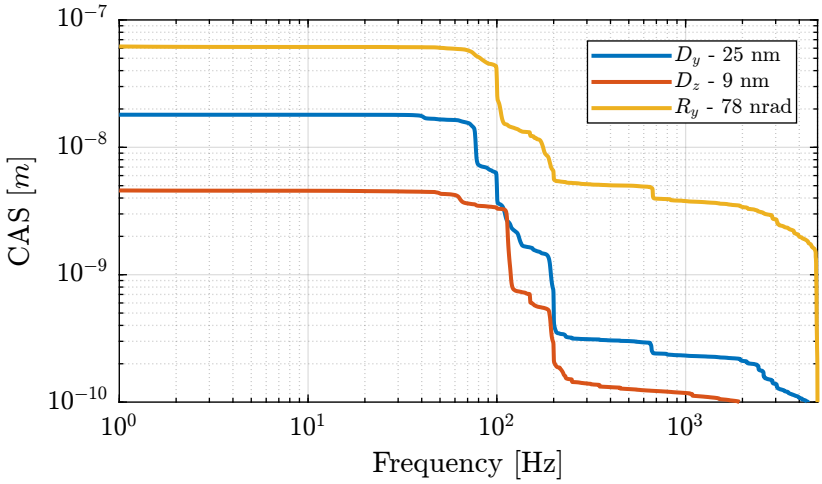

Figure 4.3: Measured vibration with the interferometers

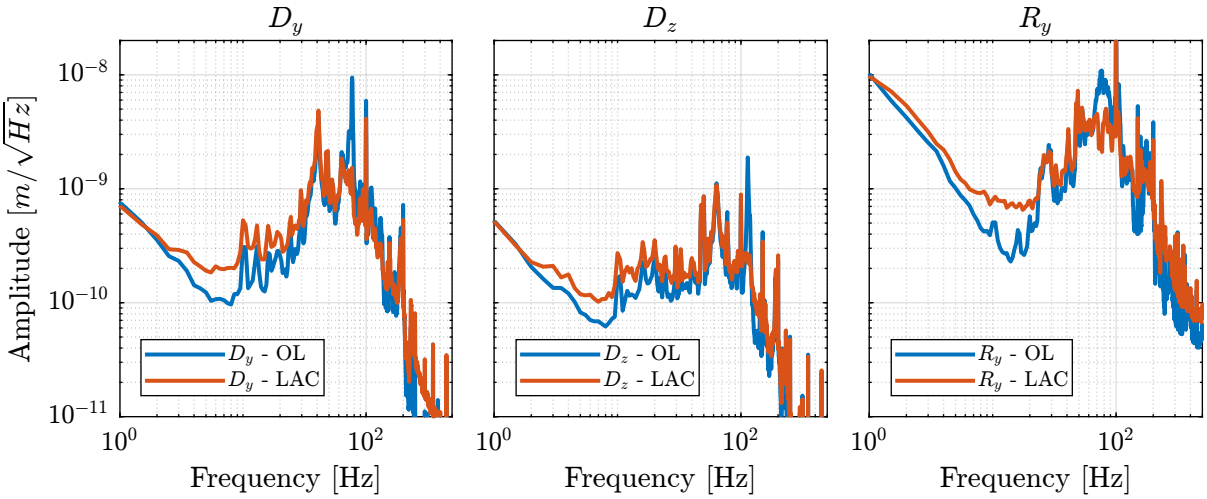

Figure 4.4: Measured vibration with the interferometers

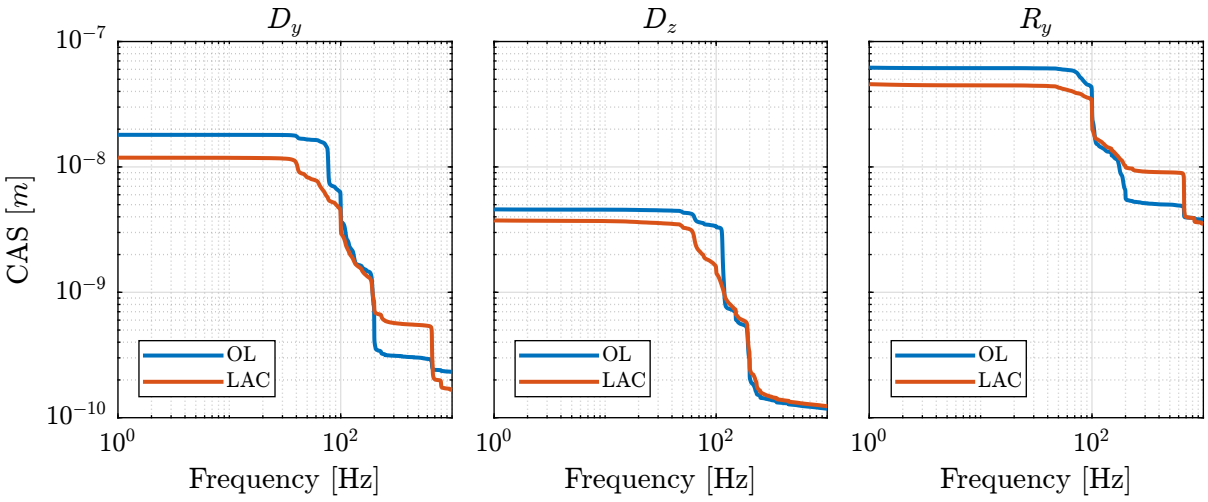

Figure 4.5: Measured vibration with the interferometers

4.3 Effect of rotation

Rotation induces lots of vibrations, especially at high velocity.

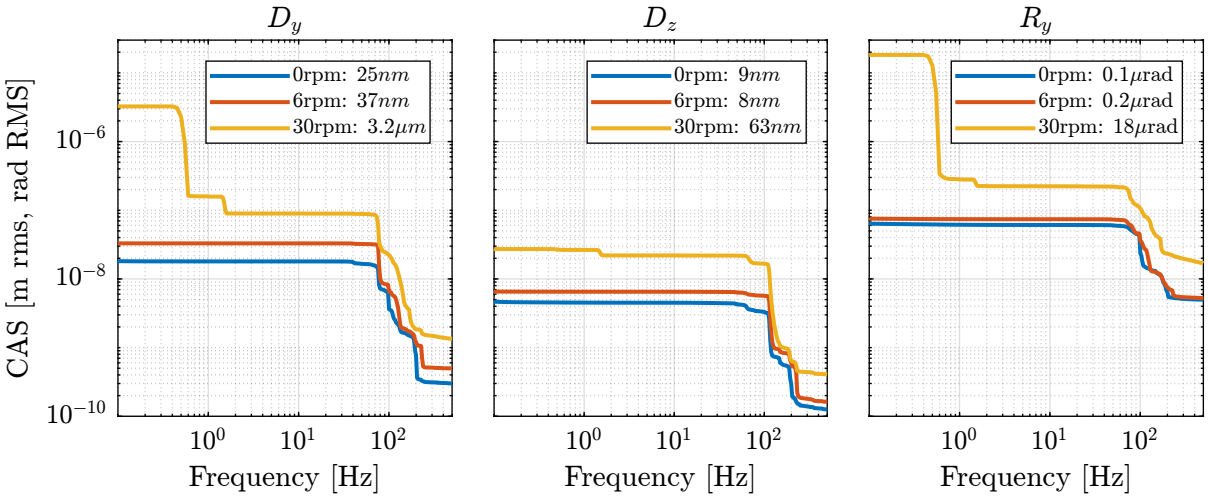

Figure 4.6: Cumulative Amplitude Spectrum for the three important directions (D_y, D_z and R_y). Three rotating velocities are shown. Integrated RMS values are shown in the legend.

4.4 Effect of HAC

Bandwidth is approximately 10Hz.

4.5 Noise coming from force sensor

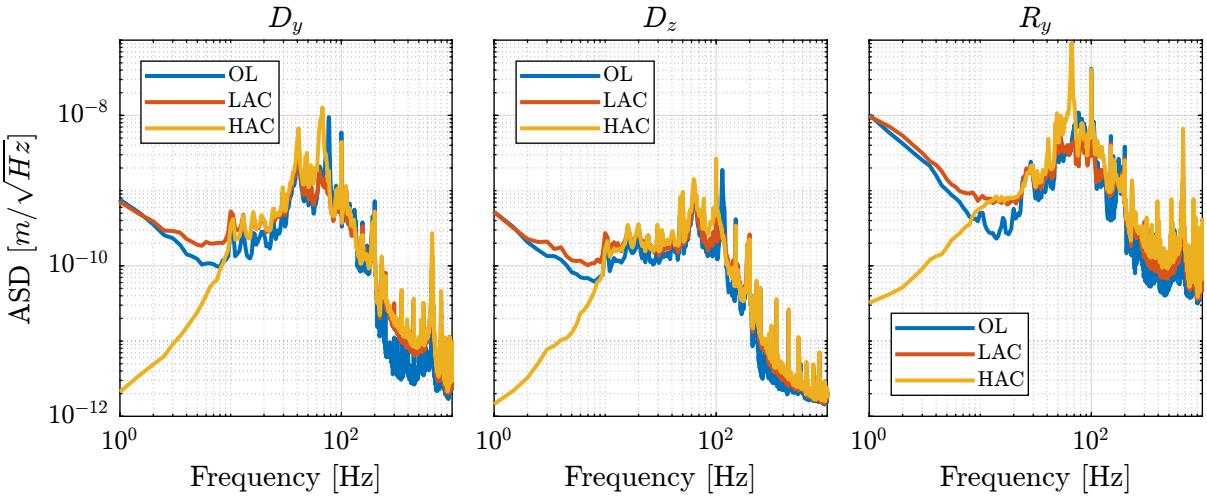

Figure 4.7: Measured vibration with the interferometers

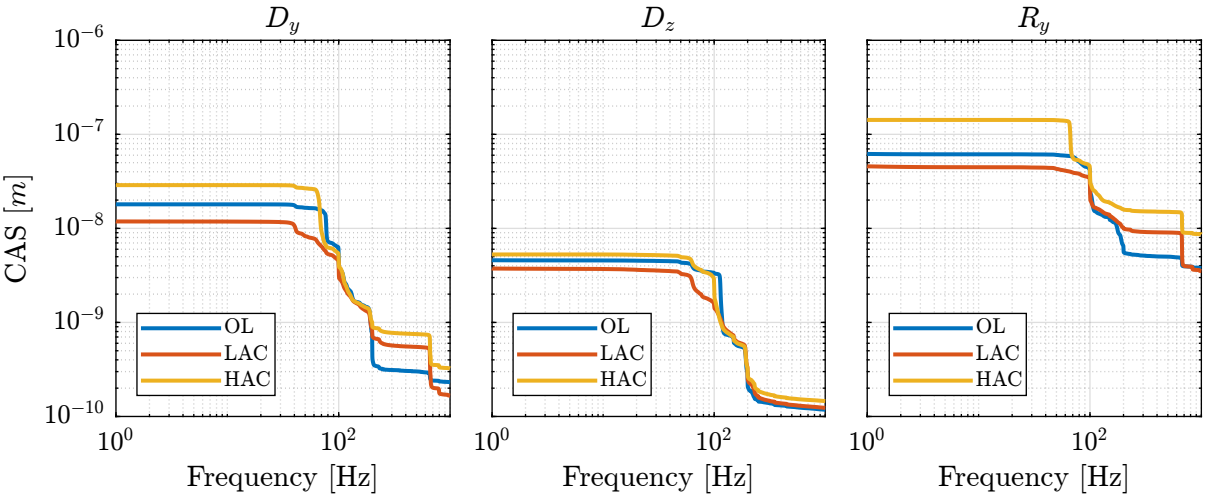

Figure 4.8: Measured vibration with the interferometers

5 Integral Force Feedback

5.1 IFF Plants

5.1.1 6x6 Plant

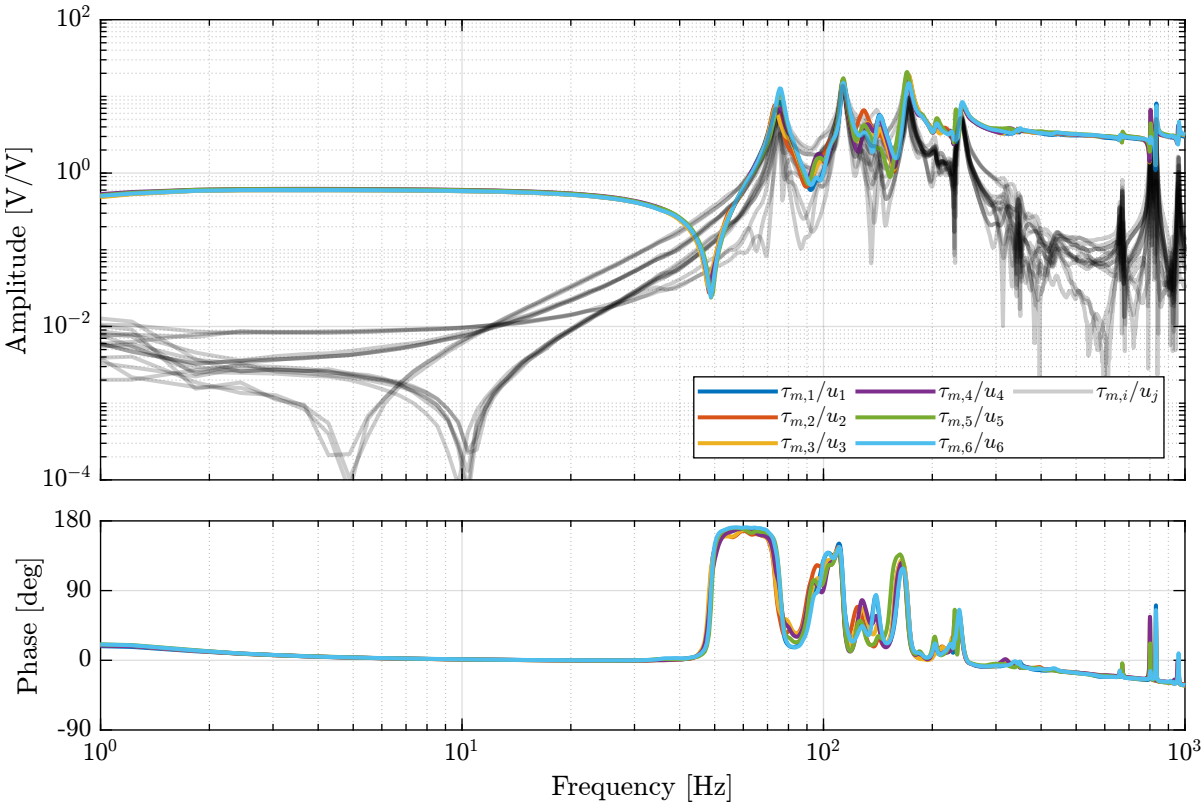

Figure 5.1: Obtained transfer function from generated voltages to measured voltages on the piezoelectric force sensor

Compare with Model:

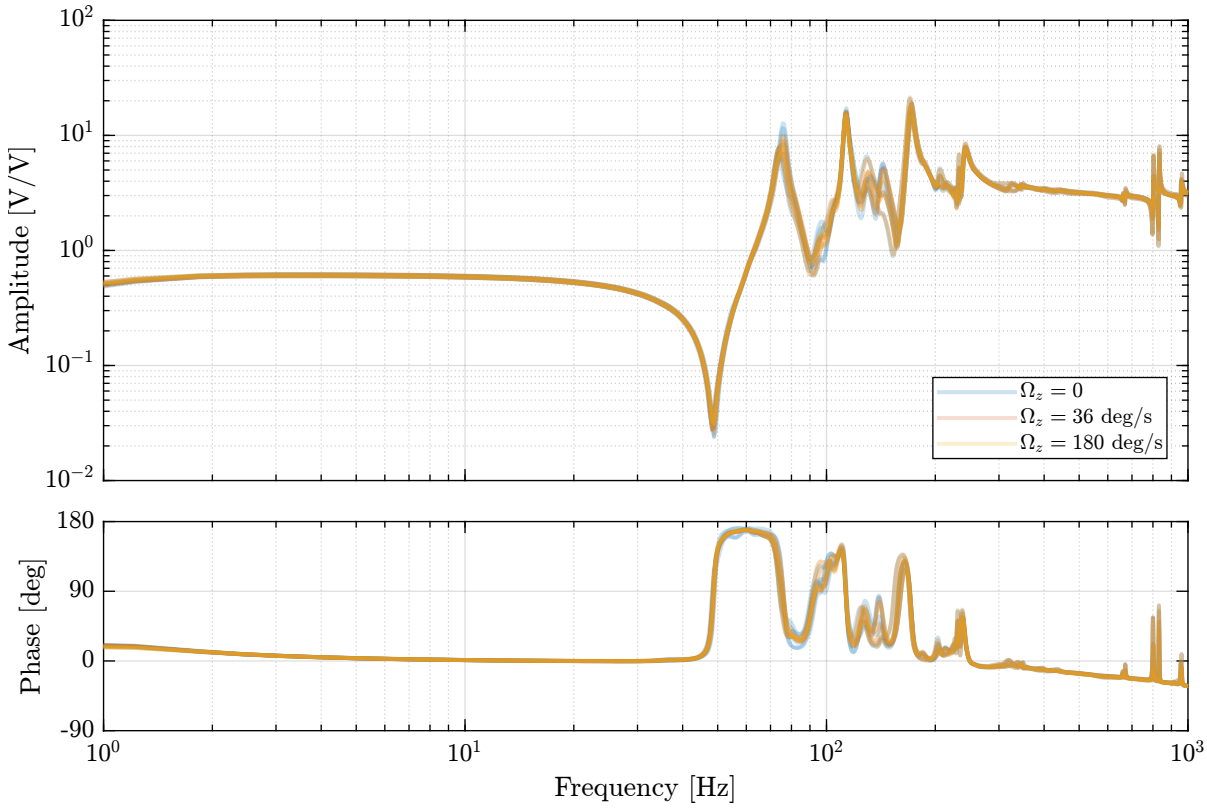

Figure 5.2: Obtained transfer function from generated voltages to measured voltages on the piezoelectric force sensor

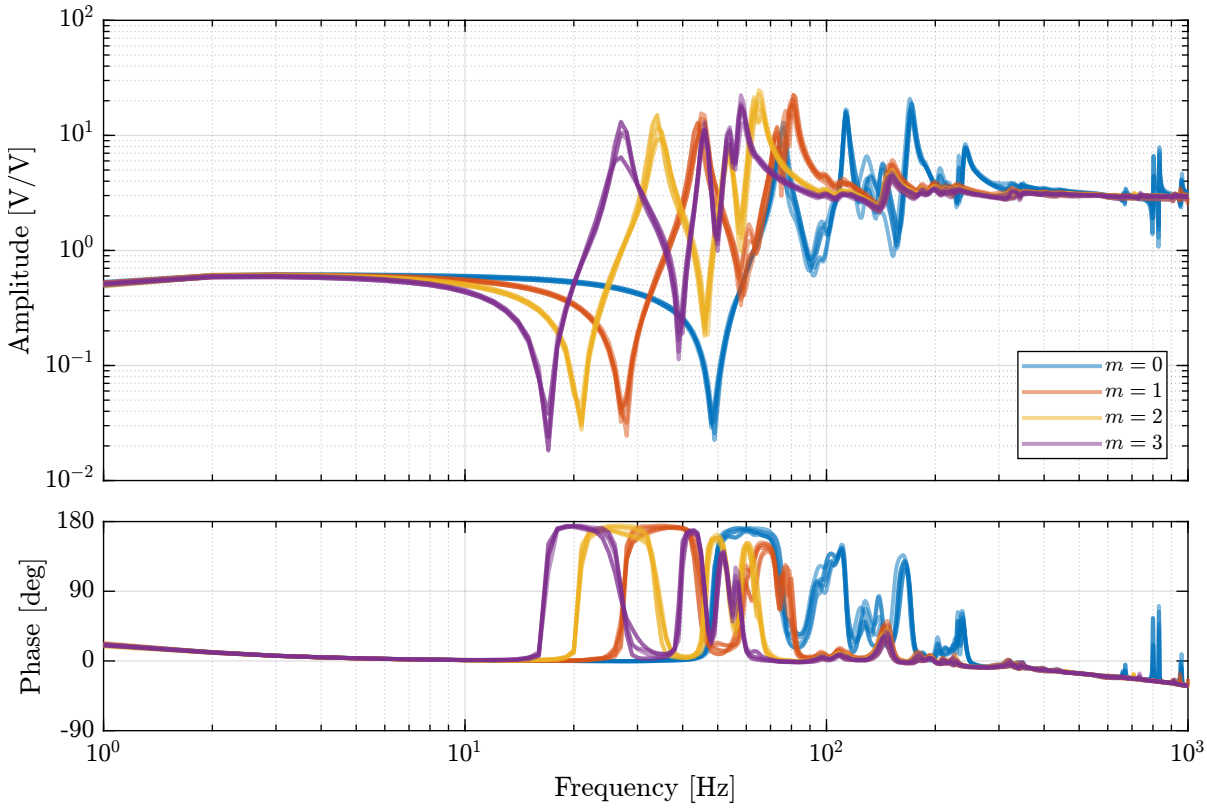

Figure 5.3: Obtained transfer function from generated voltages to measured voltages on the piezoelectric force sensor

5.1.2 Effect of Rotation

5.1.3 Effect of Mass

5.1.4 Compare with the model

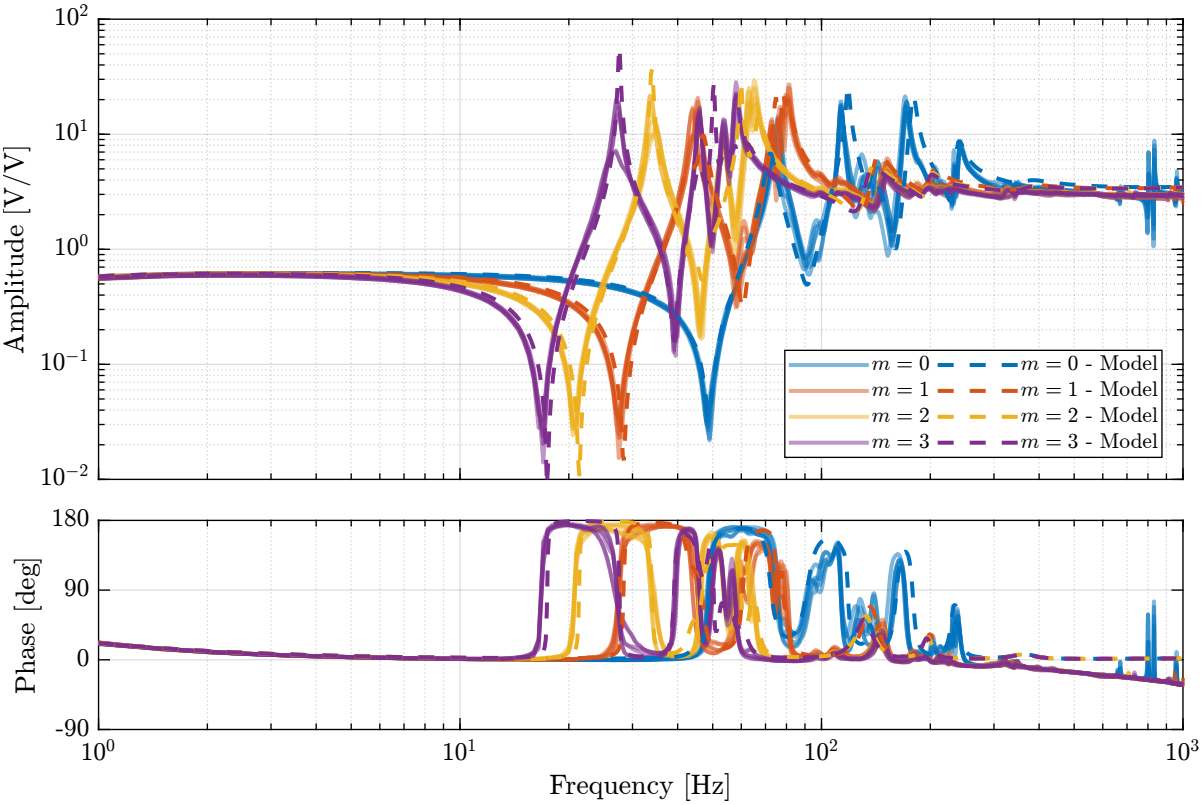

Figure 5.4: Comparison of the identified IFF plant and the IFF plant extracted from the simscape model

5.2 IFF Controller

5.2.1 Controller Design

Test second order high pass filter: We want integral action between 20Hz and 200Hz. Loop Gain:

Root Locus to obtain optimal gain.

5.2.2 Verify Stability

Verify Stability with Nyquist plot:

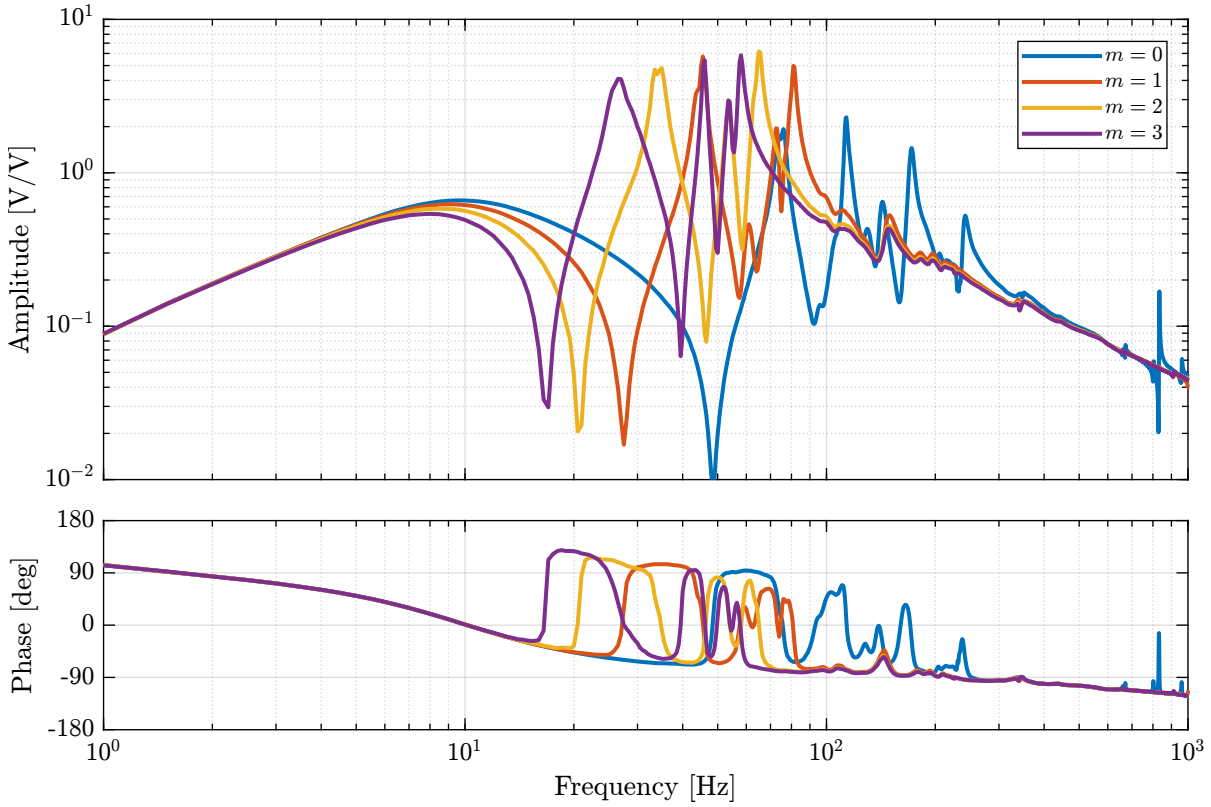

Figure 5.5: IFF Loop gain of the diagonal terms

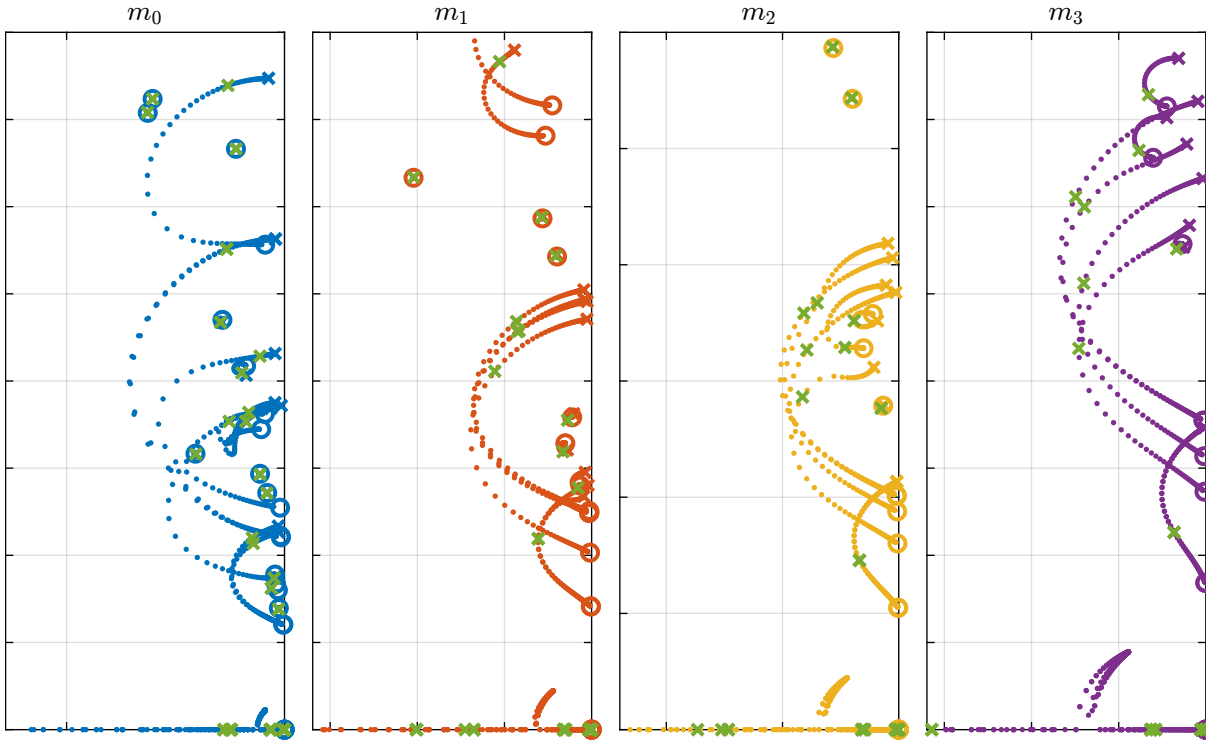

Figure 5.6: Root Locus for IFF. Green crosses are closed-loop poles for the same choosen IFF gain.

- Why bad stability margins?

5.2.3 Save Controller

5.3 Estimated Damped Plant

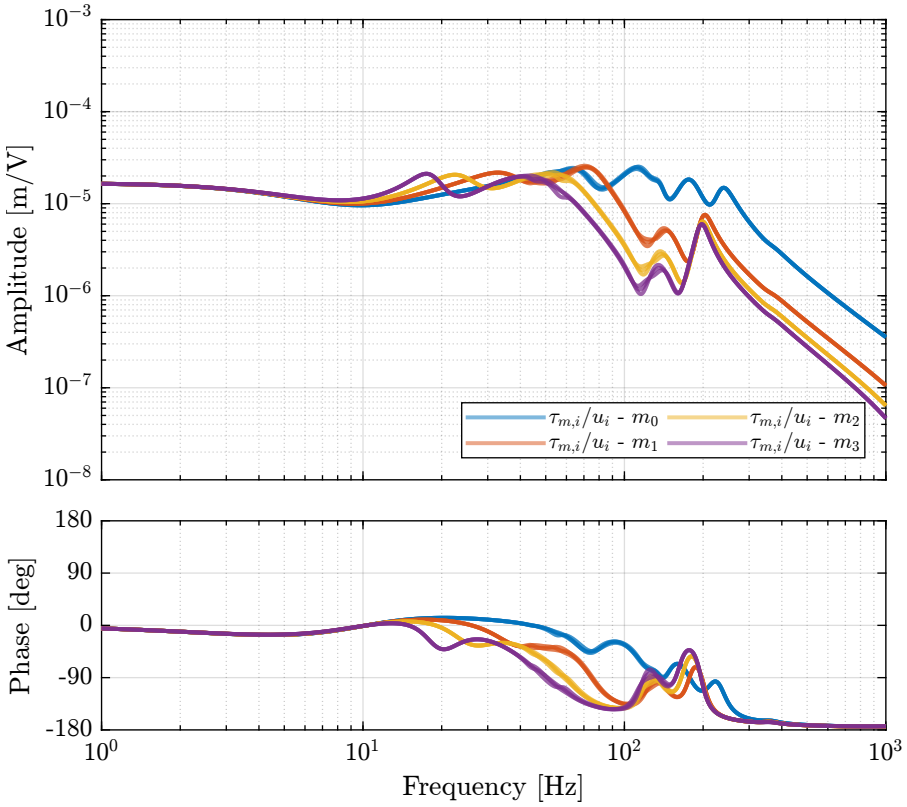

Figure 5.7: description

6 High Authority Control

6.1 Identify Spurious modes

6.2 HAC Plants

6.2.1 6x6 Plant

Compare with Model:

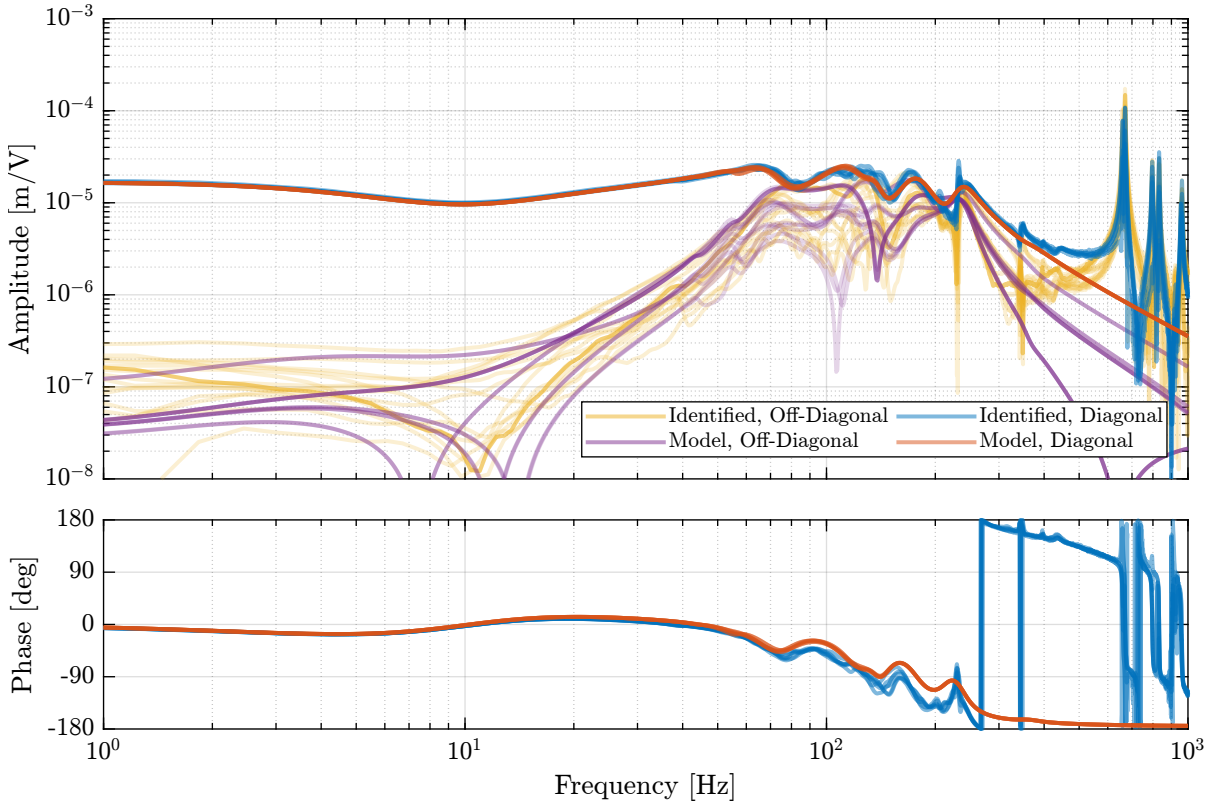

Figure 6.1: 6x6 plant from generated voltages to displacement of the struts as measured by the external metrology

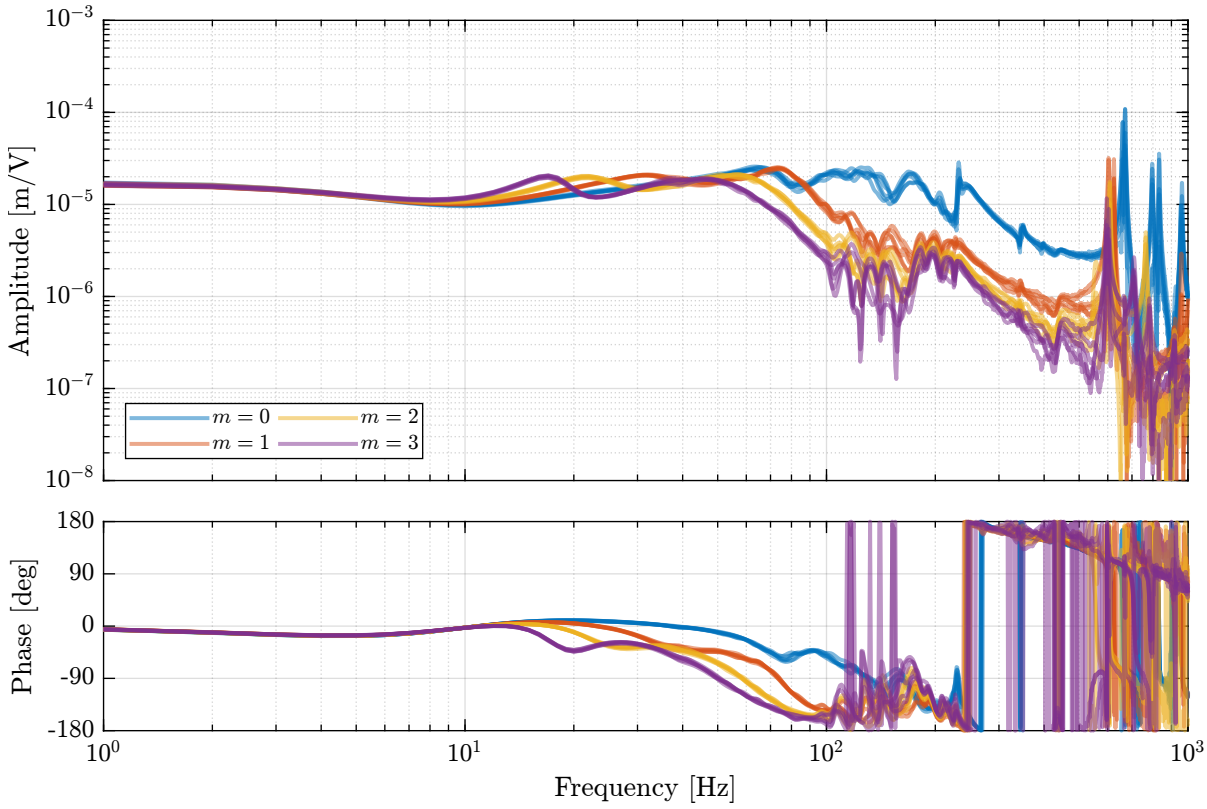

Figure 6.2: Obtained transfer function from generated voltages to measured voltages on the piezoelectric force sensor

6.2.2 Effect of Mass

6.2.3 Compare with the model

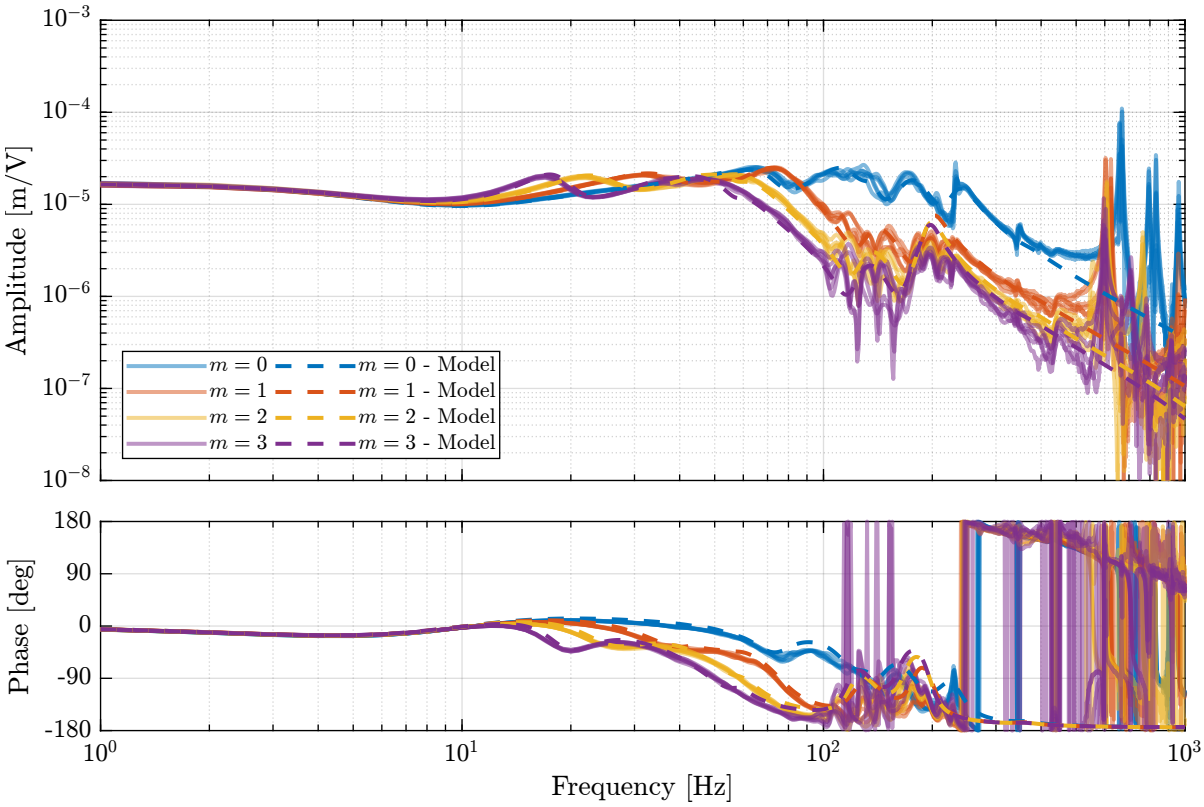

Figure 6.3: Comparison of the identified HAC plant and the HAC plant extracted from the simscape model

6.2.4 Comparison with Undamped plant

6.3 Robust HAC

6.3.1 Controller design

Loop gain

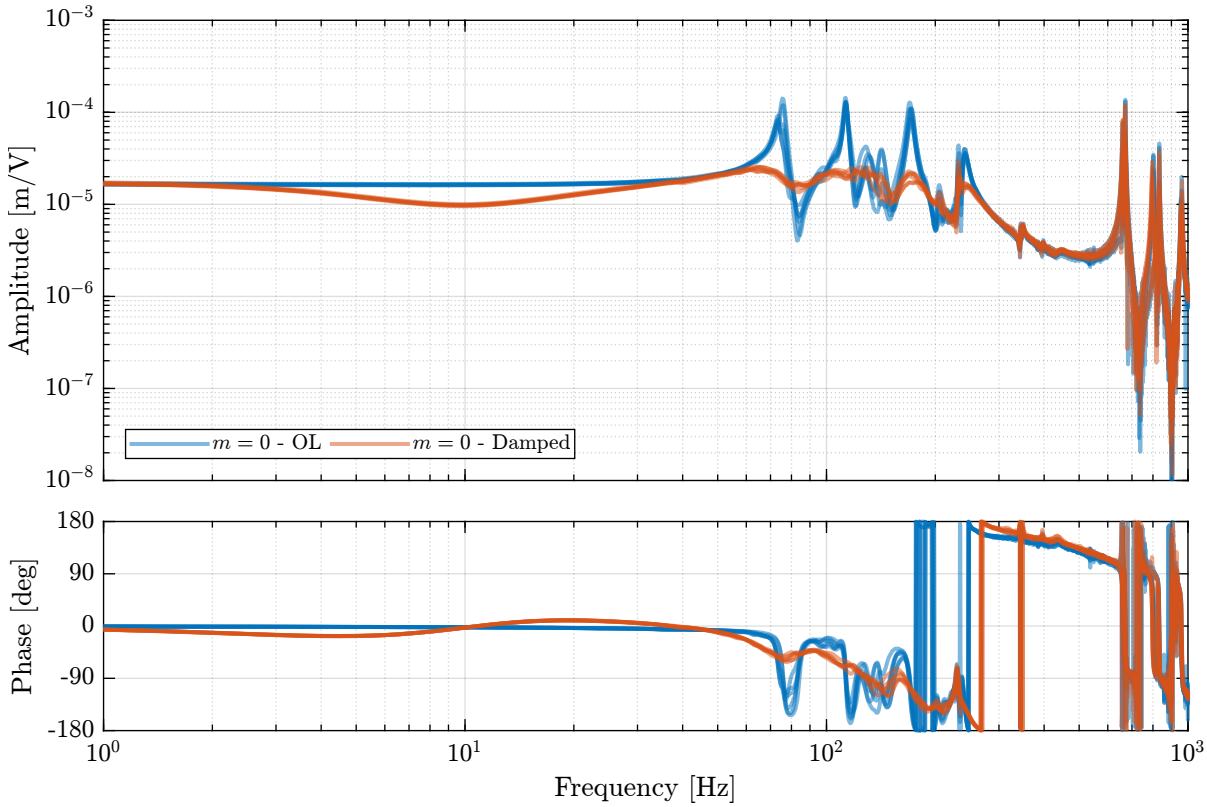

Figure 6.4: description

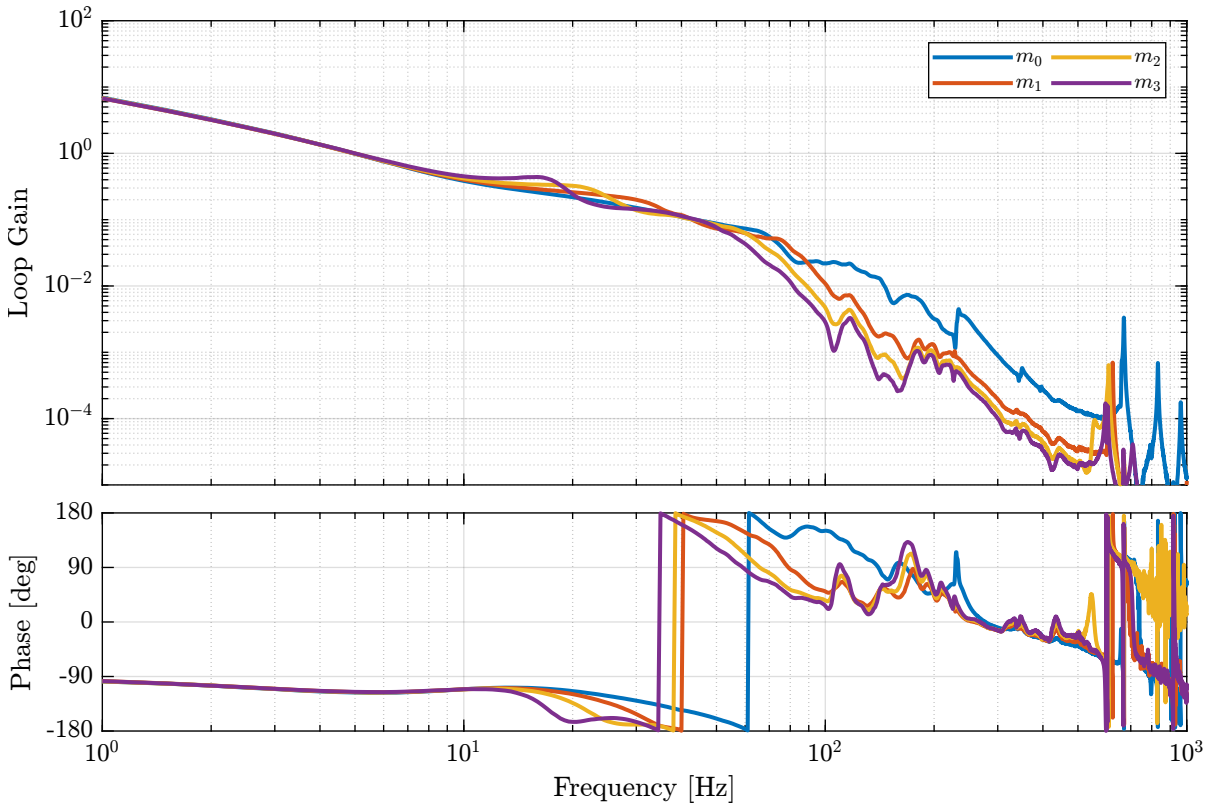

Figure 6.5: description

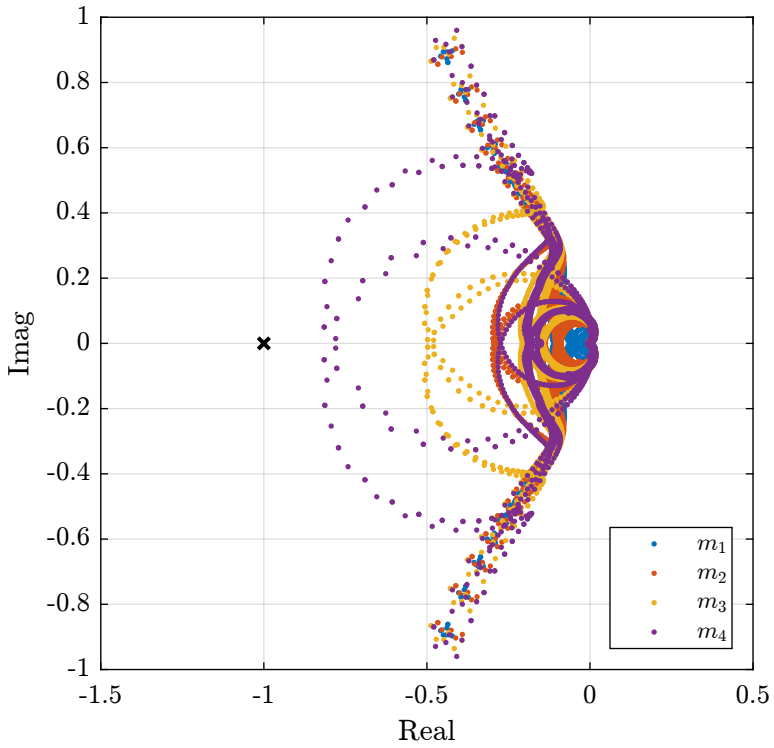

Figure 6.6: description

6.3.2 Verify Stability

6.3.3 Estimated performances

6.3.4 Save Controller

6.4 High Performance HAC

The goal is to make a controller specific for one mass in order to have high bandwidth.

6.4.1 Mass 0

Load Plant

Plant

Controller design Loop gain

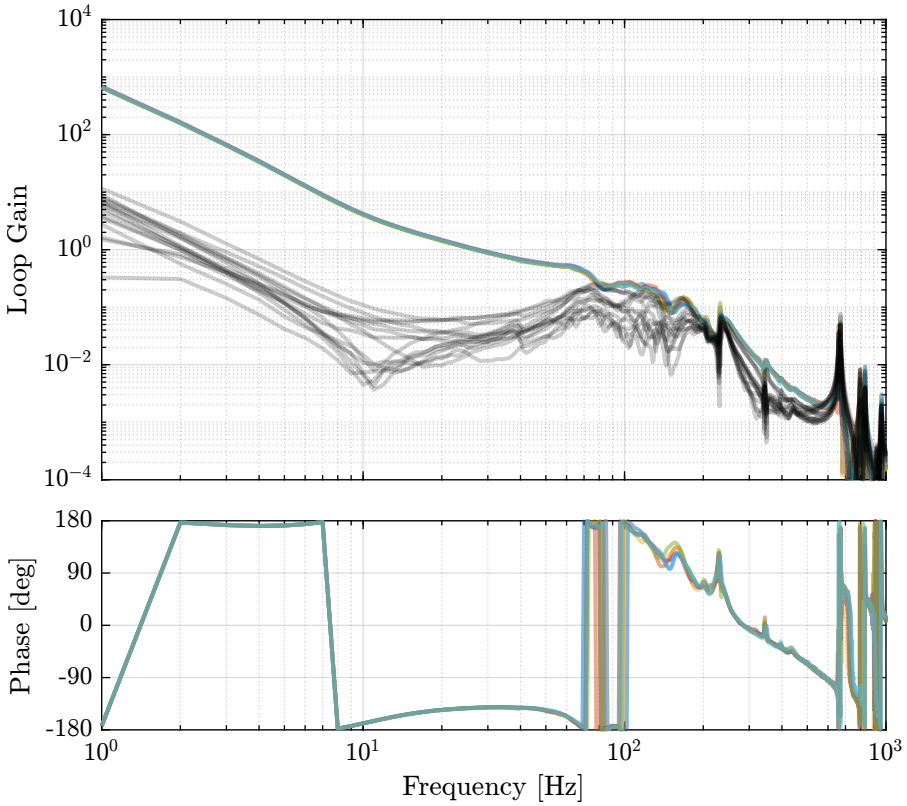

Figure 6.7: Loop gain for the High Authority Control

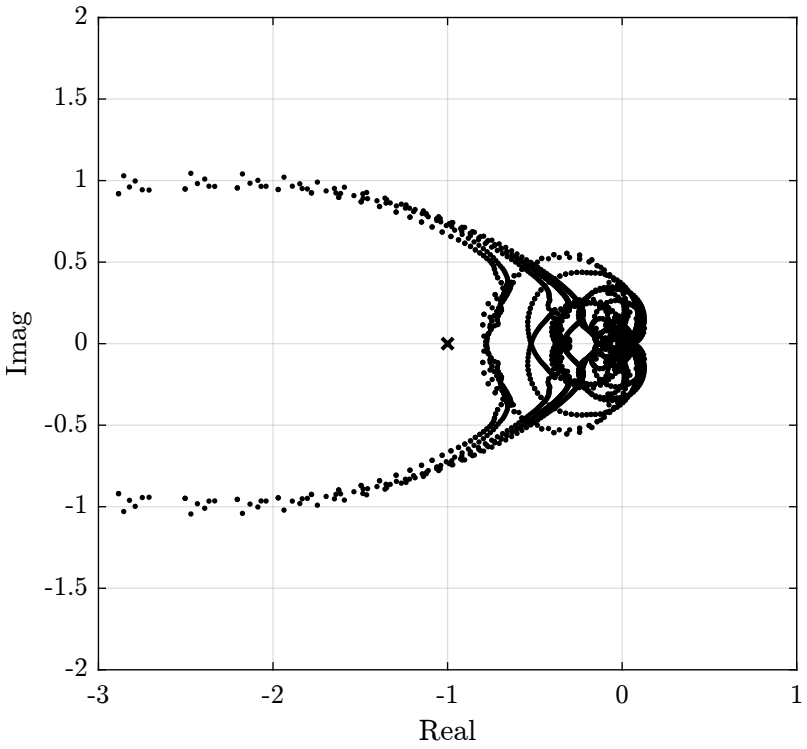

Figure 6.8: Nyquist plot for the High Authority Control

Verify Stability

Estimated performances Loop gain with model

Save Controller

Experimental Validation

	Dy [nm]	Dz [nm]	Ry [urad]
1rpm	55.3	5.9	0.1
30rpm	85.2	12.5	0.3

Closed-Loop identification

6.4.2 Mass 1

Load Plant

Plant

Plant Inverse

Controller design Loop gain

Verify Stability

Estimated performances Loop gain with model

Save Controller

6.5 Tomography - Performances

6.5.1 First scan with closed-loop at middle

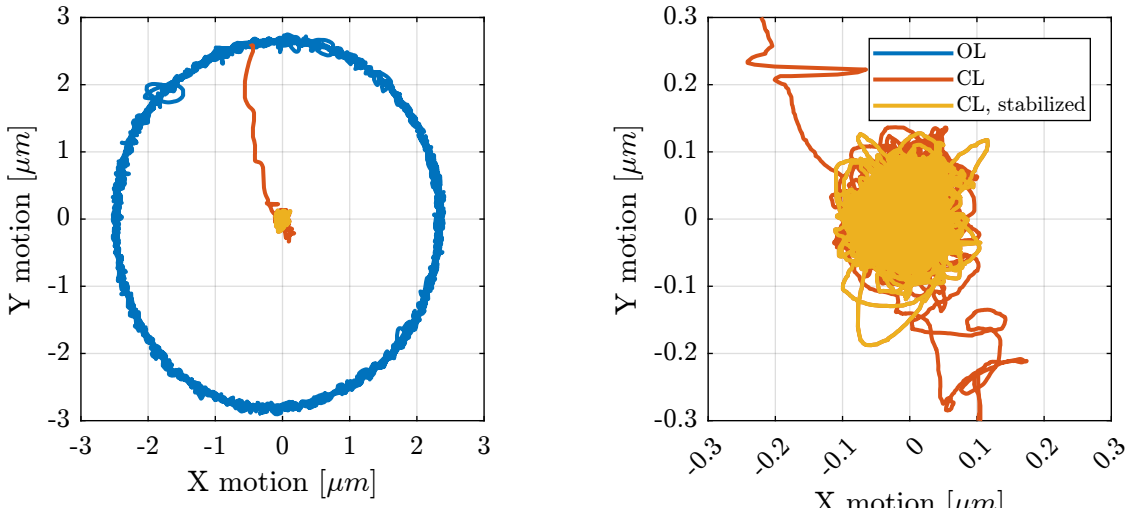

Figure 6.9: description

6.5.2 Slow Rotation - 6RPM

6.5.3 Rapid Rotation - 30RPM

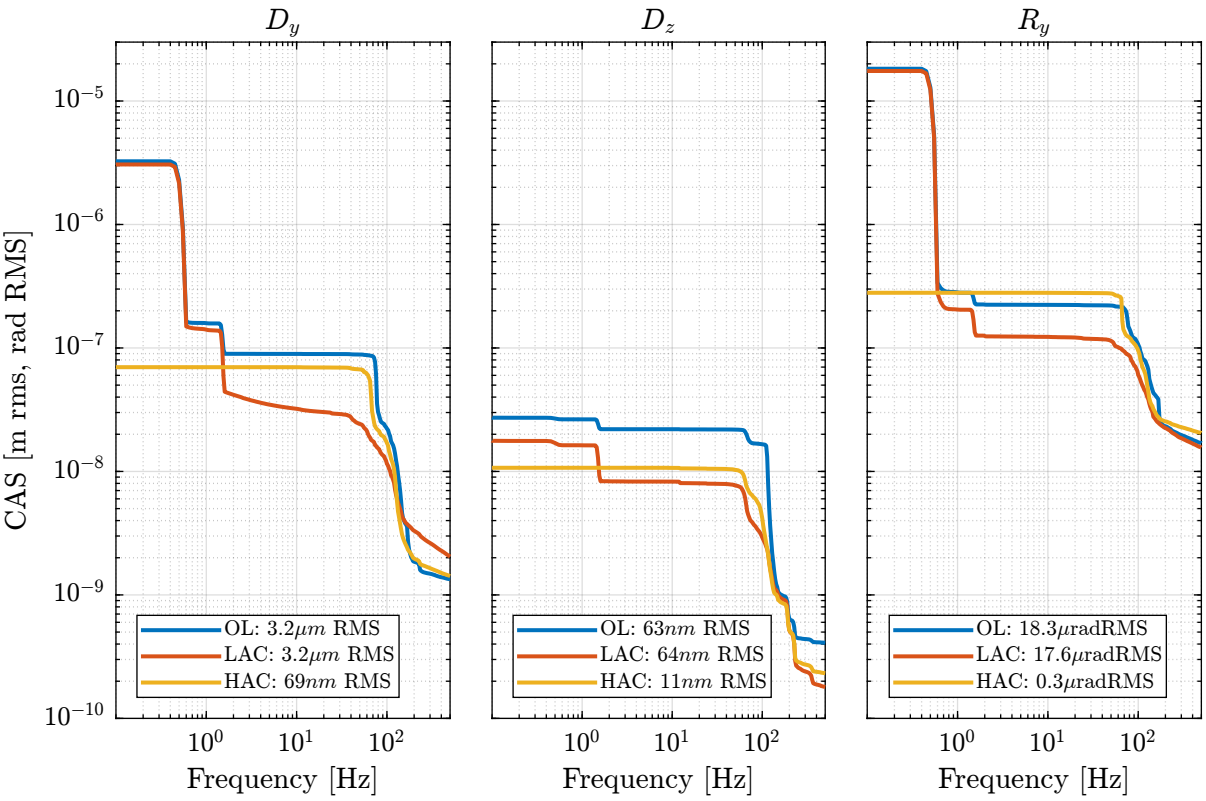

Figure 6.10: Cumulative Amplitude Spectrum of the errors in D_y, D_z and R_y during a tomography scan at 30RPM. Three control configuration are compared: Open-Loop, Low Authority Control, and High Authority Control

7 6DoF Control in Cartesian plane (rotating with the nano-hexapod)

As only Dy, Dz and Ry directions are important, we could only control them. This lead to a 3x3 plant that may be more decoupled than the 6x6 plant.

7.1 5x5 plant in Cartesian plane

Compute identified plant in the Cartesian plane: Compute plant model in the Cartesian plane:

7.2 Controller Design

7.3 Check Stability

7.4 Save controllers

7.5 Performances

2023-08-18_18-33_m0_1rpm_K_cart.mat

8 3DoF Control in Cartesian plane (fixed)

As only Dy, Dz and Ry directions are important, we could only control them. This lead to a 3x3 plant that may be more decoupled than the 6x6 plant.

8.1 3x3 plant in Cartesian plane

Compute identified plant in the Cartesian plane: Compute plant model in the Cartesian plane:

Important

Diagonal elements are matching quite well, but off-diagonal elements are very different.
Why so much more coupling than from the model?

- Is it due to the metrology? The spheres could induce coupling as for instance X motion will also be seen as Z motion. This is especially true if not well centered with the sphere (as seemed to be the case for the lateral interferometers).

Normalization of outputs:

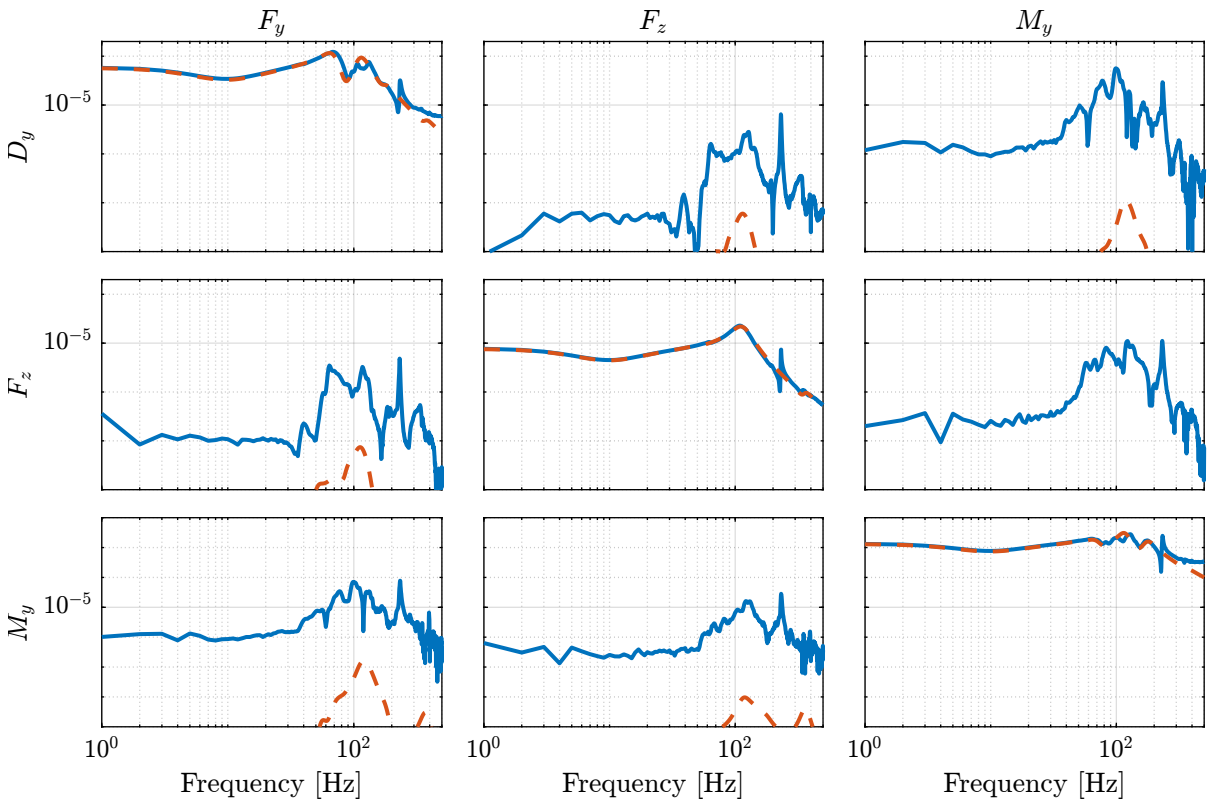

Figure 8.1: 3x3 cartesian plant

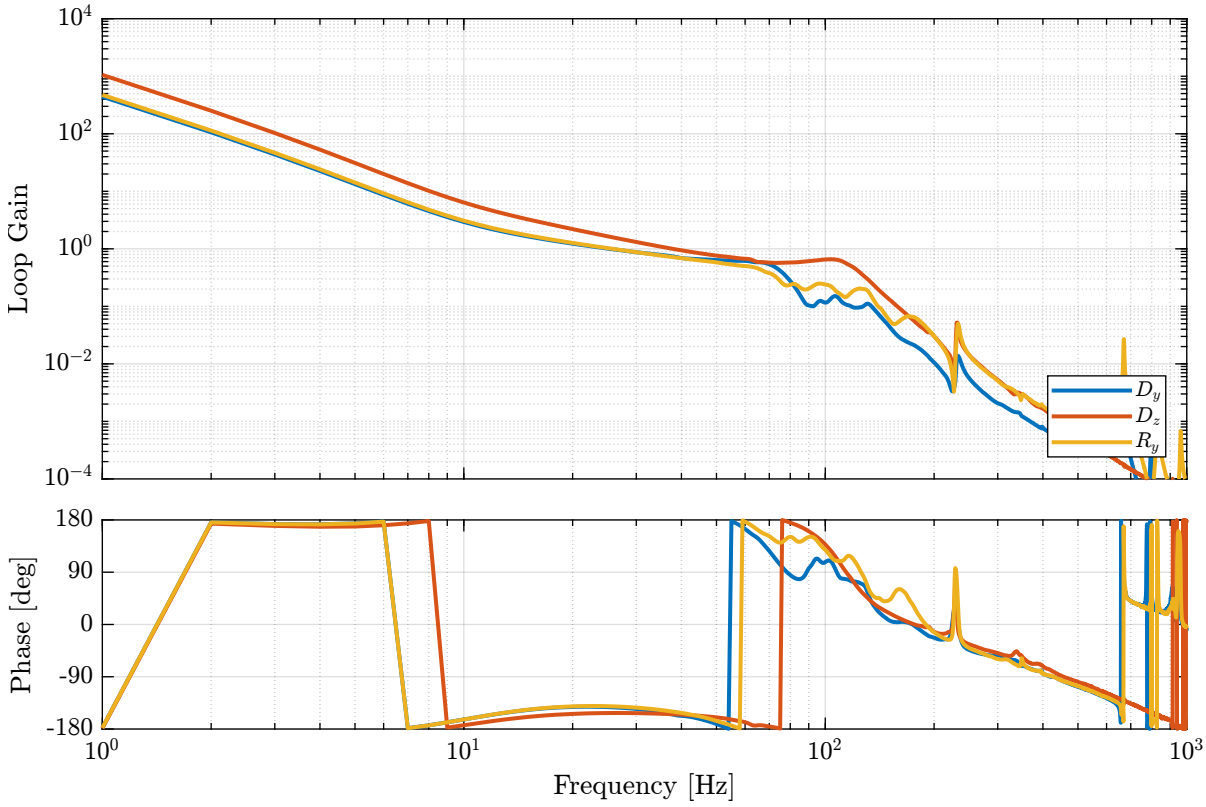

Figure 8.2: description

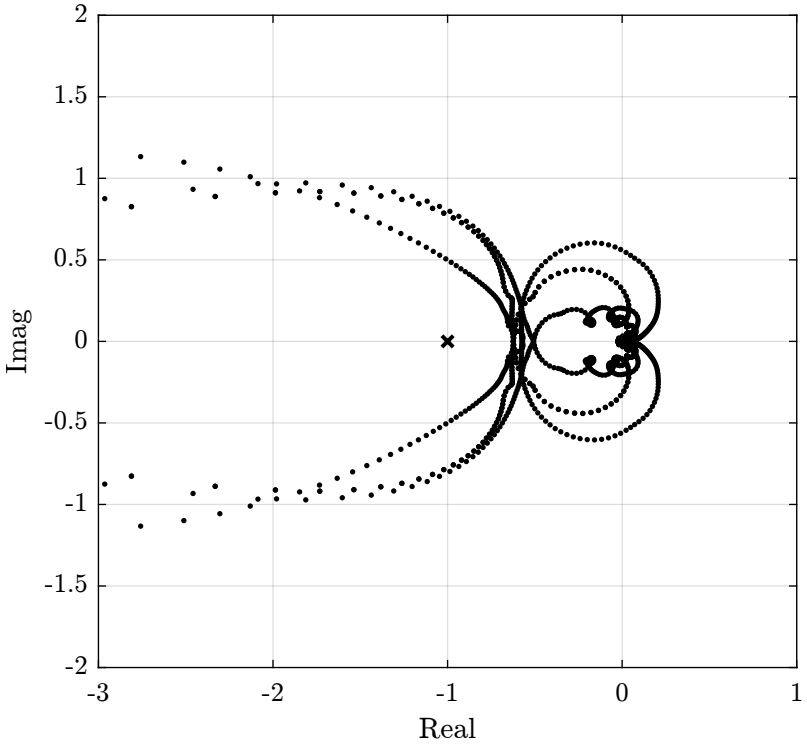

Figure 8.3: description

8.2 Controller Design

8.2.1 Dy

8.2.2 Dz

8.2.3 Ry

8.2.4 3x3 controller

8.3 Check Stability

8.4 Save controllers

8.4.1 Save Controller

8.5 Controller Design (normalized)

8.6 Verify Stability

8.7 Control Performances

Compare with estimated performances

9 Complementary Filter Control

9.1 m0

9.1.1 3x3 plant in Cartesian plane

Compute identified plant in the Cartesian plane: Compute plant model in the Cartesian plane:

9.1.2 Plant Invert

Reduce model size Add first resonance

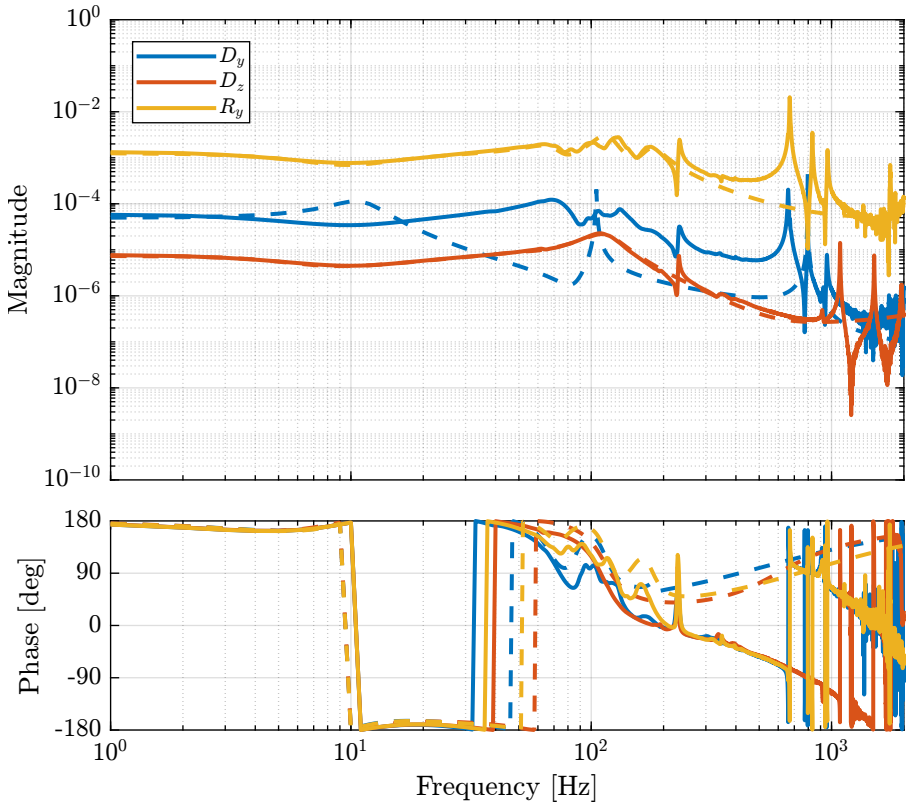

Figure 9.1: Comparaison of the measured direct terms and the reduced order models

Invert and make realizable

9.1.3 Save Plant Inverse

9.1.4 Control Performances

5Hz

Compare with estimated performances

20Hz

Compare with estimated performances

Different bandwidth for different directions

Compare with estimated performances

Dz 25Hz

Compare with estimated performances

9.1.5 Better plant invert

Dy Stable Inverse

Dz Stable Inverse

Ry Stable Inverse

Compare Invert plants

Save plant inverse

Compare Digital Invert plants

9.1.6 Control Performances

Better plant invert

9.1.7 Scans with good controller

1rpm 1RPM scans are performed for all the masses with the same controller.

	Dx [nm]	Dy [nm]	Dz [nm]	Rx [nrad]	Ry [nrad]
m0	796	20	8	8209	73

30rpm 1RPM scans are performed for all the masses with the same controller.

	Dx [nm]	Dy [nm]	Dz [nm]	Rx [nrad]	Ry [nrad]
m0	820	39	13	7790	156

9.2 m1

9.2.1 3x3 plant in Cartesian plane

Compute identified plant in the Cartesian plane: Compute plant model in the Cartesian plane: Normalization of outputs:

9.2.2 Better plant invert

Dy Stable Inverse

Dz Stable Inverse

Ry Stable Inverse

Compare Invert plants

Save plant inverse

Compare Digital Invert plants

9.2.3 Control Performances

Better plant invert

9.2.4 Scans with good controller

1rpm 1RPM scans are performed for all the masses with the same controller.

	Dx [nm]	Dy [nm]	Dz [nm]	Rx [nrad]	Ry [nrad]
m0	796	20	8	8209	73

30rpm 1RPM scans are performed for all the masses with the same controller.

	Dx [nm]	Dy [nm]	Dz [nm]	Rx [nrad]	Ry [nrad]
m0	820	39	13	7790	156

9.3 m2

9.3.1 3x3 plant in Cartesian plane

Compute identified plant in the Cartesian plane: Compute plant model in the Cartesian plane: Normalization of outputs:

9.3.2 Better plant invert

Dy Stable Inverse

Dz Stable Inverse

Ry Stable Inverse

Compare Invert plants

Save plant inverse

Compare Digital Invert plants

9.3.3 Control Performances

Better plant invert

9.3.4 Scans with good controller

1rpm 1RPM scans are performed for all the masses with the same controller.

	Dx [nm]	Dy [nm]	Dz [nm]	Rx [nrad]	Ry [nrad]
m0	796	20	8	8209	73

30rpm 1RPM scans are performed for all the masses with the same controller.

	Dx [nm]	Dy [nm]	Dz [nm]	Rx [nrad]	Ry [nrad]
m0	820	39	13	7790	156

9.4 m3

9.4.1 3x3 plant in Cartesian plane

Compute identified plant in the Cartesian plane: Compute plant model in the Cartesian plane: Normalization of outputs:

9.4.2 Better plant invert

Dy Stable Inverse

Dz Stable Inverse

Ry Stable Inverse

Compare Invert plants

Save plant inverse

Compare Digital Invert plants

9.4.3 Control Performances

Better plant invert

9.4.4 Scans with good controller

1rpm 1RPM scans are performed for all the masses with the same controller.

	Dx [nm]	Dy [nm]	Dz [nm]	Rx [nrad]	Ry [nrad]
m0	796	20	8	8209	73

30rpm 1RPM scans are performed for all the masses with the same controller.

	Dx [nm]	Dy [nm]	Dz [nm]	Rx [nrad]	Ry [nrad]
m0	820	39	13	7790	156

10 Scans

- Section 10.1
- Section 10.2
- Section 10.3
- Section 10.4
- Section 10.5

10.1 R_z scans: Tomography

m0: 30rpm, 6rpm, 1rpm m1: 6rpm, 1rpm m2: 6rpm, 1rpm m3: 1rpm

10.1.1 Robust Control - 1rpm

1RPM scans are performed for all the masses with the same robust controller.

The problem for these scans is that the position initialization was not make properly, so the open-loop errors are quite large (see Figure 10.1).

The obtained open-loop and closed-loop errors are shown in tables 10.1 and 10.2 respectively.

Table 10.1: Measured error during open-loop tomography scans (1rpm)

	D_x $[\mu m]$	D_y $[\mu m]$	D_z $[nm]$	R_x [μrad]	R_y [μrad]
m_0	6	6	32	34	34
m_1	6	7	26	51	55
m_2	36	38	36	259	253
m_3	31	33	38	214	203

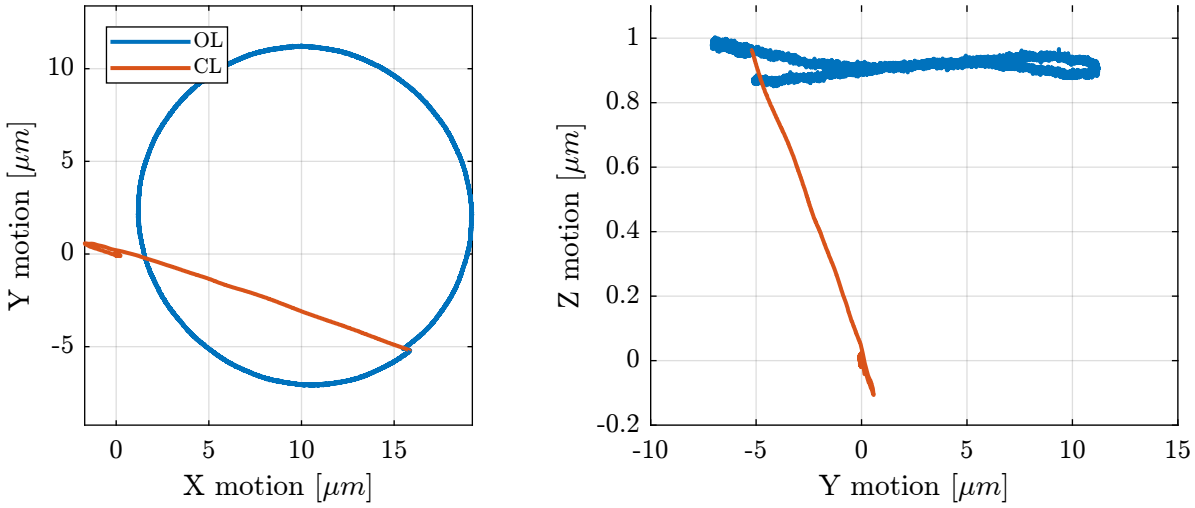

Figure 10.1: D_x, D_y and D_z motion during a slow (1RPM) tomography experiment. Open Loop data is shown in blue and closed-loop data in red

Table 10.2: Measured error during closed-loop tomography scans (1rpm, robust controller)

	D_x [nm]	D_y [nm]	D_z [nm]	R_x [nrad]	R_y [nrad]
m_0	13	15	5	57	55
m_1	16	25	6	102	55
m_2	25	25	7	120	103
m_3	40	53	9	225	169

Table 10.3: Measured error during open-loop tomography scans (6rpm)

	D_x [μm]	D_y [μm]	D_z [nm]	R_x [μrad]	R_y [μrad]
m_0	8	7	20	41	41
m_1	4	4	21	39	39

Table 10.4: Measured error during closed-loop tomography scans (6rpm, robust controller)

	D_x [nm]	D_y [nm]	D_z [nm]	R_x [nrad]	R_y [nrad]
m_0	17	19	5	70	73
m_1	20	26	7	110	77

Table 10.5: Measured error during open-loop tomography scans (30rpm)

	D_x [μm]	D_y [μm]	D_z [nm]	R_x [μrad]	R_y [μrad]
m_0	2	2	24	10	10

Table 10.6: Measured error during closed-loop tomography scans (30rpm, robust controller)

	D_x [nm]	D_y [nm]	D_z [nm]	R_x [nrad]	R_y [nrad]
m_0	34	38	10	127	129

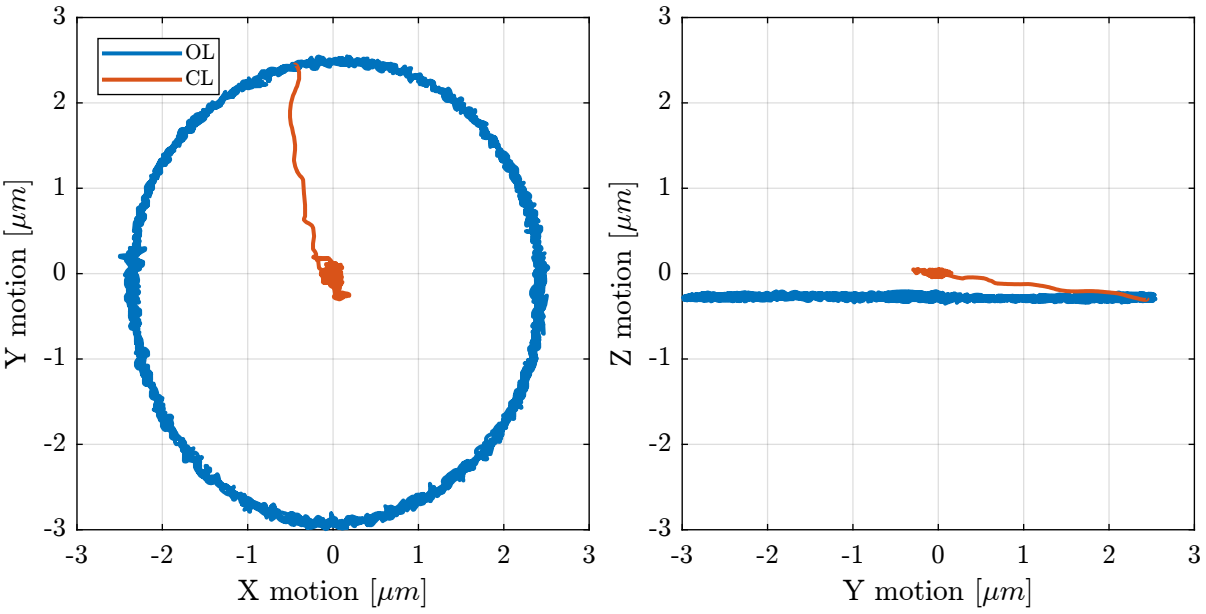

Figure 10.2: Measured motion during tomography scan at 30RPM with a robust controller

10.1.2 Robust Control - 6rpm

10.1.3 Robust Control - 30rpm

10.2 D_z scans: Dirty Layer Scans

10.2.1 Step by Step D_z motion

Three step sizes are tested:

- 10 nm steps (Figure 10.3)
- 100 nm steps (Figure 10.4)
- 1 μm steps (Figure 10.5)

10.2.2 Continuous D_z motion: Dirty Layer Scans

Two D_z scans are performed:

- at 10 $\mu m/s$ in Figure 10.6
- at 100 $\mu m/s$ in Figure 10.7

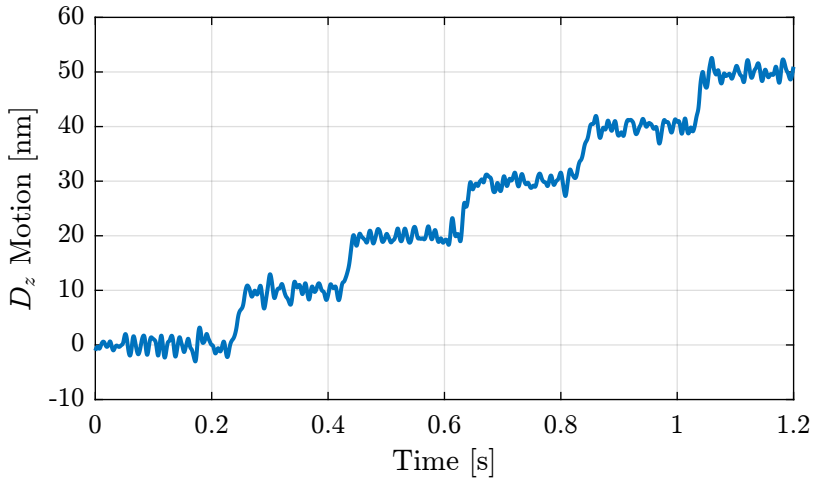

Figure 10.3: Dz MIM test with 10nm steps (low pass filter with cut-off frequency of 10Hz is applied)

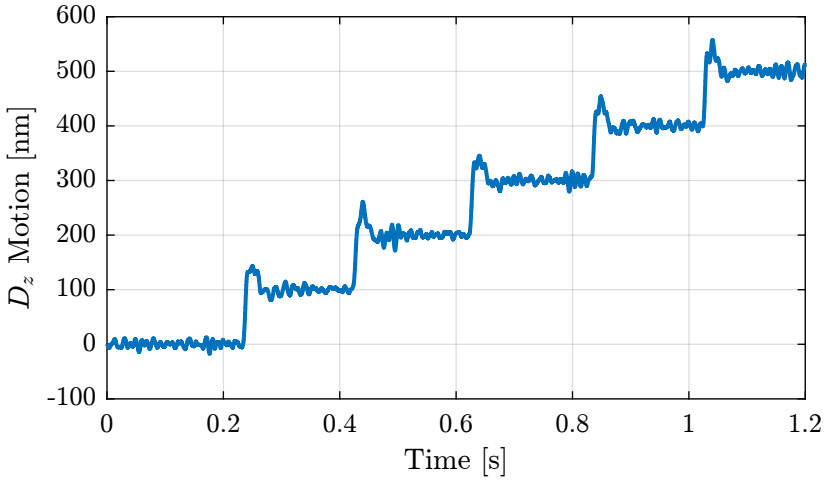

Figure 10.4: Dz MIM test with 100nm steps

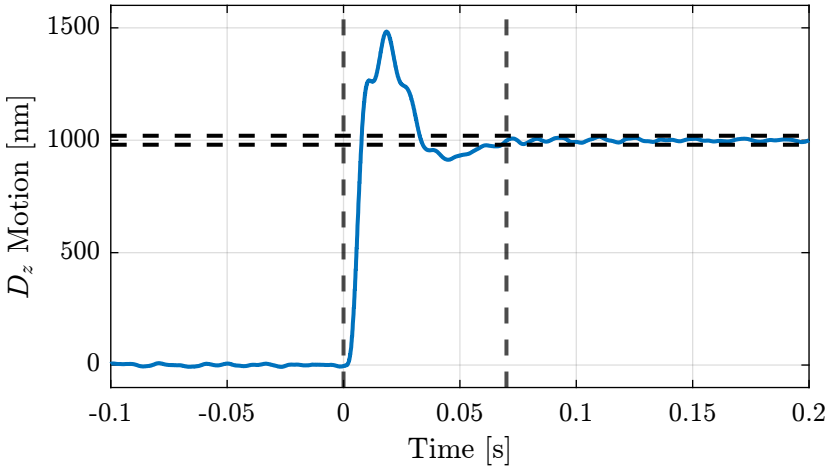

Figure 10.5: D_z step response - Stabilization time is around 70ms

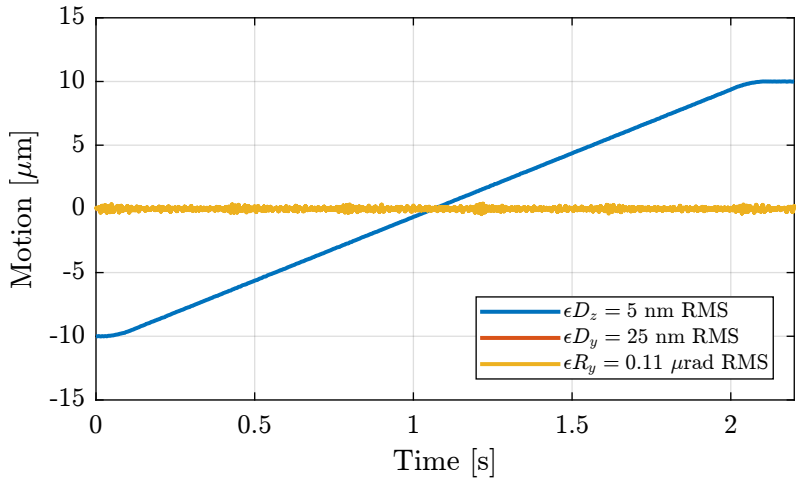

Figure 10.6: Dirty layer scan: D_z motion at $10\,\mu m/s$

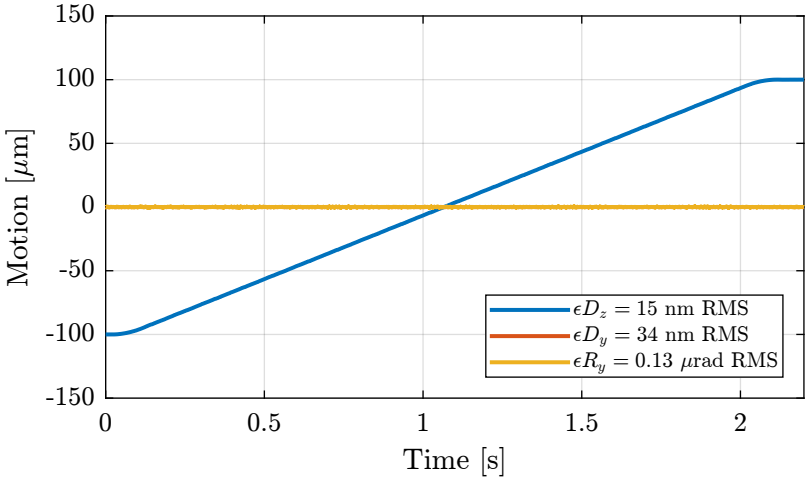

Figure 10.7: Dirty layer scan: D_z motion at $100\,\mu m/s$

10.3 R_y scans: Reflectivity

An R_y scan is performed at $100\,\mu rad/s$ velocity (Figure 10.8). During the R_y scan, the errors in D_y are D_z are kept small.

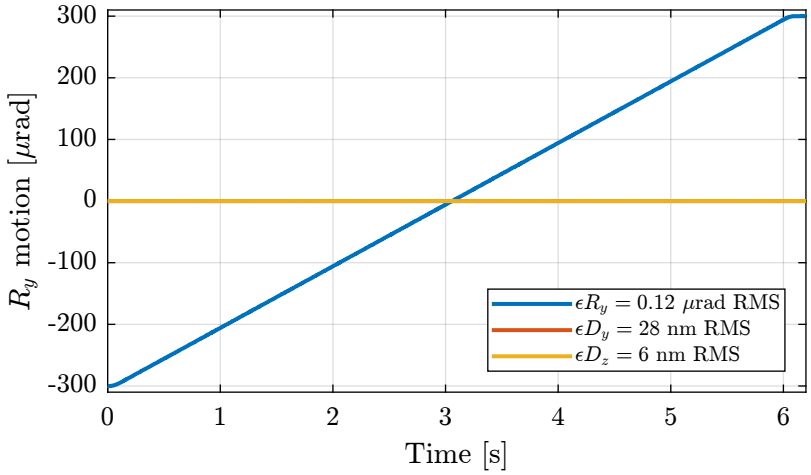

Figure 10.8: R_y reflecitivity scan at $100\,\mu\text{rad}/s$ velocity

10.4 D_y Scans

The steps generated by the IcePAP for the T_y stage are send to the Speedgoat. Then, we can know in real time what is the wanted position in D_y during T_y scans.

10.4.1 Open Loop

We can clearly see micro-stepping errors of the stepper motor used for the T_y stage. The errors have a period of $10\,\mu m$ with an amplitude of $\pm 100\,nm$.

10.4.2 Closed Loop

10.4.3 Faster Scan

Because of micro-stepping errors of the Ty stepper motor, when scanning at high velocity this induce high frequency vibration that are outside the bandwidth of the feedback controller.

At $100\,\mu m/s$, the micro-stepping errors with a period of $10\,\mu m$ (see Figure 10.9) are at 10Hz. These errors are them amplified by some resonances in the system.

This could be easily solved by changing the stepper motor for a torque motor for instance.

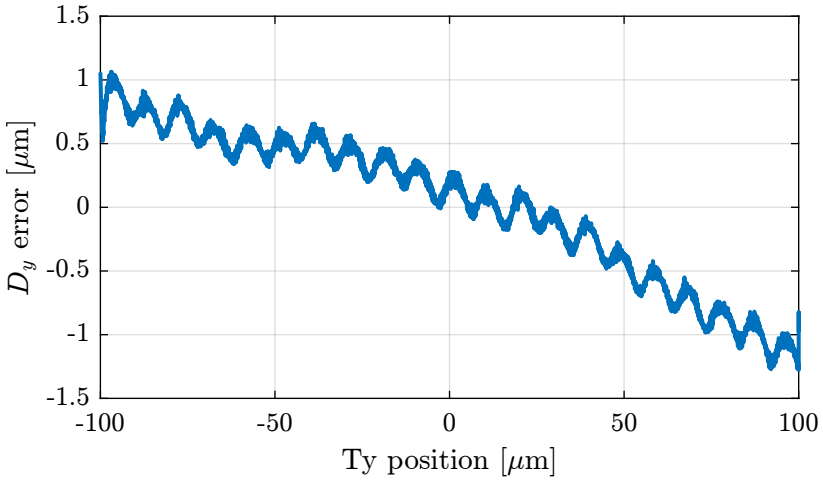

Figure 10.9: T_y scan (at $10\,\mu m/s$) - D_y errors. The micro-stepping errors can clearly be seen with a period of $10\,\mu m$ and an amplitude of $\pm 100\,nm$

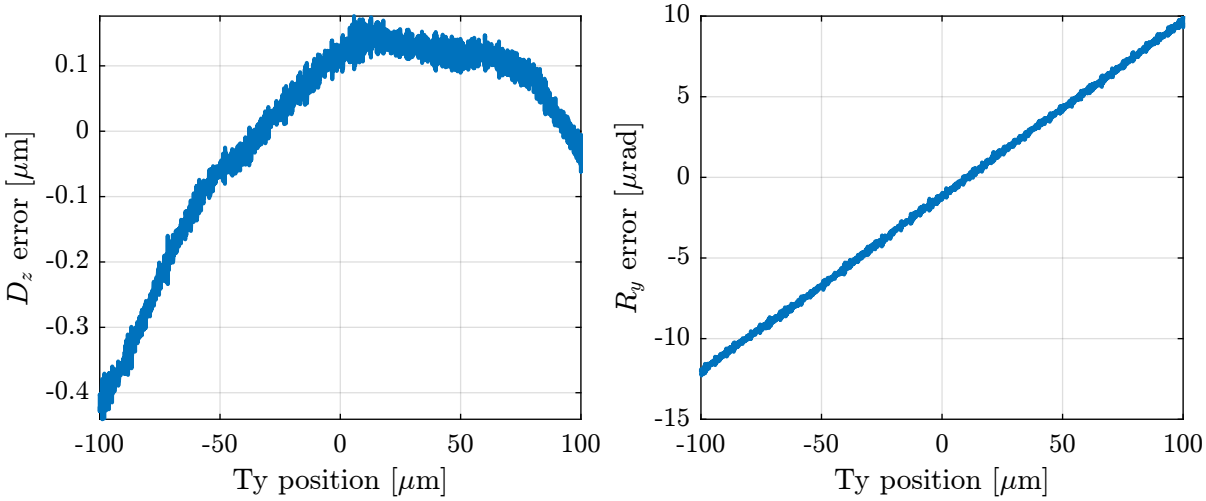

Figure 10.10: T_y scan (at $10\,\mu m/s$) - D_z and R_y errors. The D_z error is most likely due to having the top interferometer pointing to a sphere. The large R_y errors might also be due to the metrology system

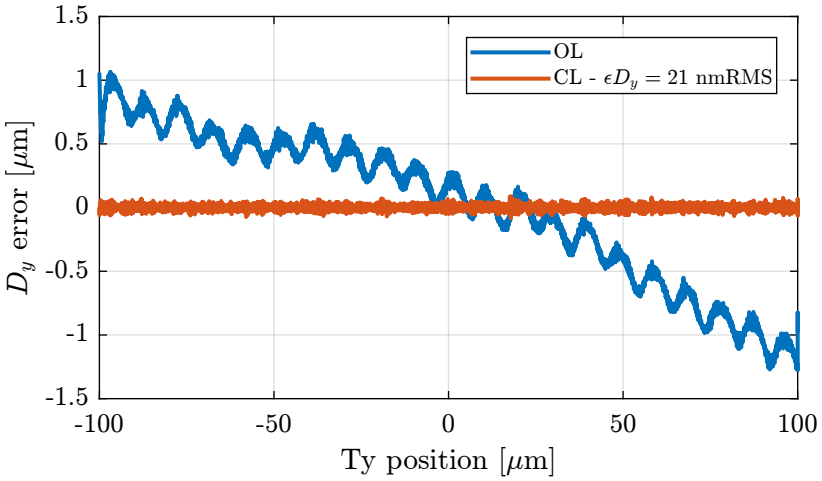

Figure 10.11: T_y scan (at $10\,\mu m/s$) - D_y errors. Open-loop and Closed-loop scans

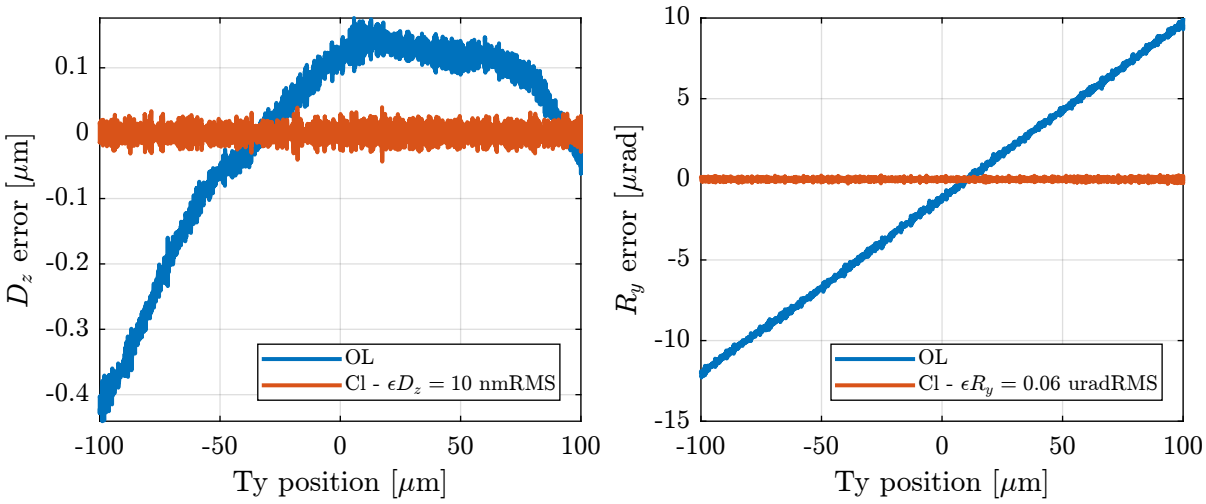

Figure 10.12: T_y scan (at $10\,\mu m/s$) - D_z and R_y errors. Open-loop and Closed-loop scans

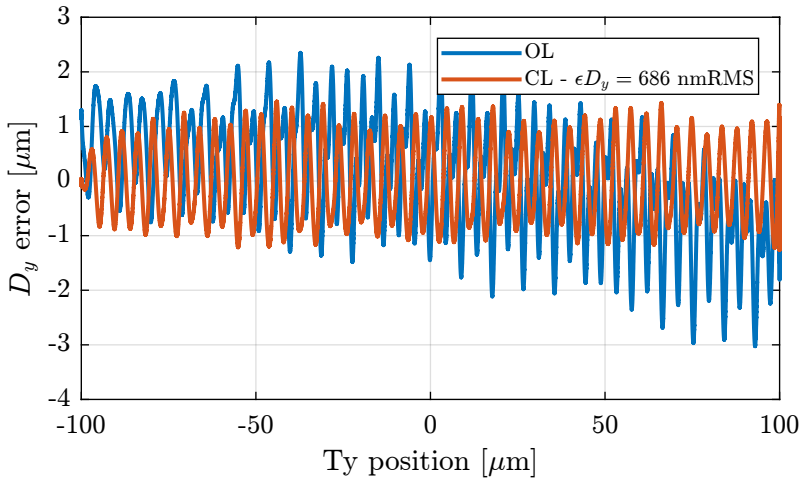

Figure 10.13: T_y scan (at $100\,\mu m/s$) - D_y errors. Open-loop and Closed-loop scans

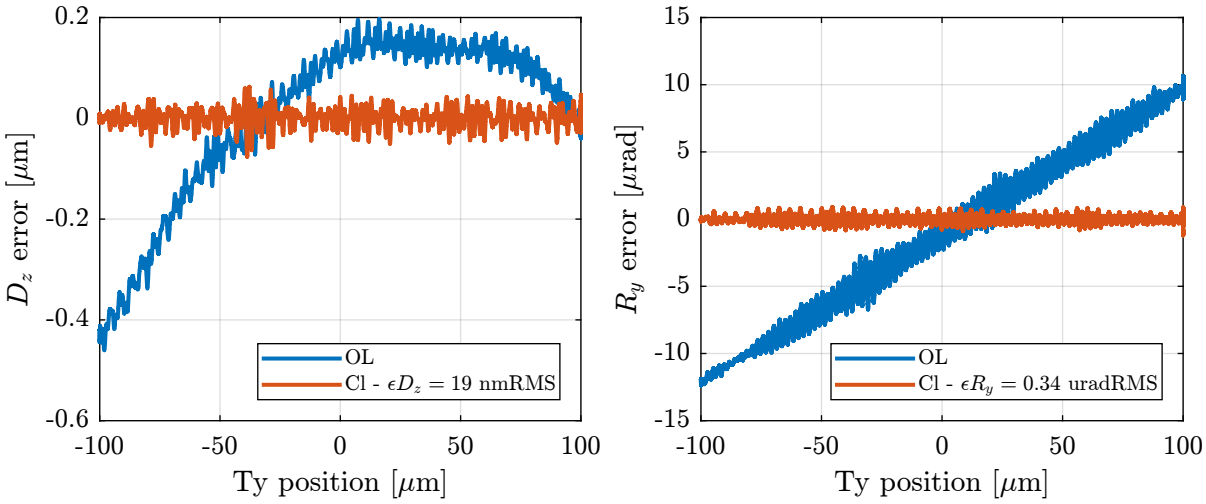

Figure 10.14: T_y scan (at $100\,\mu m/s$) - D_z and R_y errors. Open-loop and Closed-loop scans

10.5 Combined R_z and D_y: Diffraction Tomography

Instead of doing a fast R_z motion a slow D_y, the idea is to perform slow R_z (here 1rpm) and fast D_y scans with the nano-hexapod.

Here, the D_y scans are performed only with the nano-hexapod (the Ty stage is not moving), so we are limited to $\pm 100\,\mu m$.

Several D_y velocities are tested: $0.1\,mm/s$, $0.5\,mm/s$, $1\,mm/s$ and $10\,mm/s$ (see Figure 10.15).

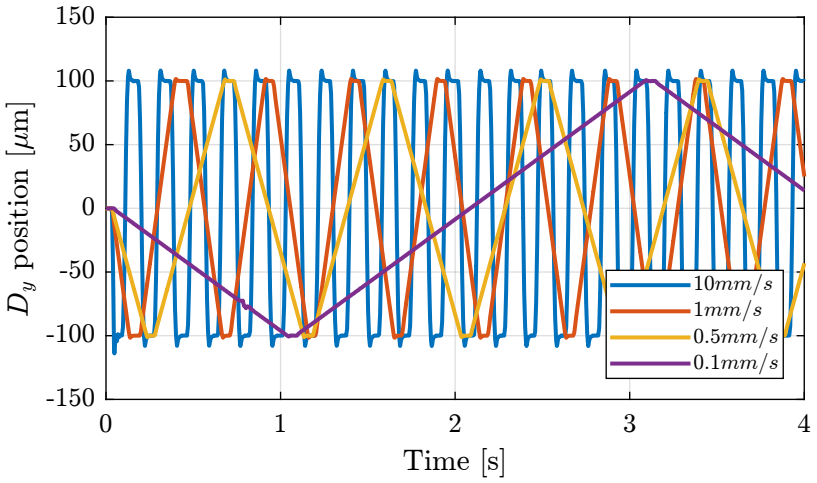

Figure 10.15: Dy motion for several configured velocities

The corresponding "repetition rate" and D_y scan per spindle turn are shown in Table 10.7.

The main issue here is the "waiting" time between two scans that is in the order of 50ms. By removing this waiting time (fairly easily), we can double the repetition rate at 10mm/s.

Table 10.7: D_y scaning repetition rate

D_y Velocity	Repetition rate	Scans per turn (at 1RPM)
0.1 mm/s	4 s	15
0.5 mm/s	0.9 s	65
1 mm/s	0.5 s	120
10 mm/s	0.18 s	330

The scan results for a velocity of 1mm/s is shown in Figure 10.16. The D_z and R_y errors are quite small during the scan.

The D_y errors are quite large as the velocity is increased. This type of scan can probably be massively improved by using feed-forward and optimizing the trajectory. Also, if the detectors are triggered in position (the Speedgoat could generate an encoder signal for instance), we don't care about the D_y errors.

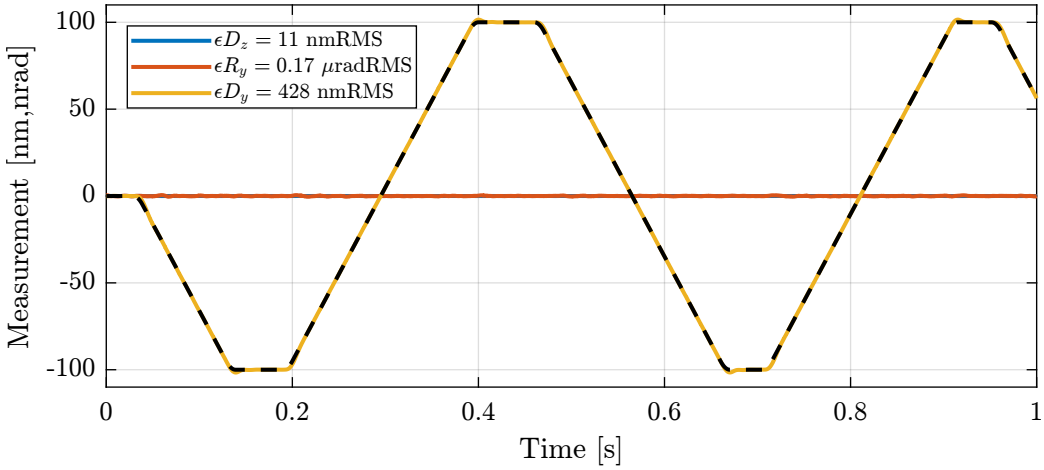

Figure 10.16: Diffraction tomography with Dy velocity of 1mm/s and Rz velocity of 1RPM

10.6 Summary of experiments

For each conducted experiments, the D_y, D_z and R_y errors are computed and summarized in Table 10.9.

Table 10.8: Obtained errors for several D_y velocities

Velocity	D_y [nmRMS]	D_z [nmRMS]
R_y [μradRMS]		
0.1 mm/s	75.5	9.1
0.1		
0.5 mm/s	190.5	10.0
0.1		
1 mm/s	428.0	11.2
0.2		
10 mm/s	4639.9	55.9
1.4		

Table 10.9: Table caption

	D_y [nmRMS]	D_z [nmRMS]	R_y [nradRMS]
Tomography (R_z 1rpm)	15	5	55
Tomography (R_z 6rpm)	19	5	73
Tomography (R_z 30rpm)	38	10	129
Dirty Layer (D_z 10 $\mu m/s$)	25	5	114
Dirty Layer (D_z 100 $\mu m/s$)	34	15	130
Reflectivity (R_y 100 μrad/s)	28	6	118
Lateral Scan (D_y 10 $\mu m/s$)	21	10	37
Diffraction Tomography (R_z 1rpm, D_y 0.1mm/s)	75	9	118
Diffraction Tomography (R_z 1rpm, D_y 1mm/s)	428	11	169